The rotational spectrum of HD broadened by H2 at temperatures between 100 – 296 K

Keeyoon Sung, Edward Wishnow, Brian Drouin, Laurent Manceron, Marine Verseils, D. Chris Benner, Conor Nixon

Highlights:

- New measurements of HD and HD-H_2 mixtures over the 50—360 cm^{-1} range, at temperatures 98-296 K, at pressures ≤ 1 bar.
- The R(0)—R(3) rotational transitions are observed in very high resolution spectra that were acquired using the AILES beam line at the Synchrotron SOLEIL, France.
- Spectroscopic line parameters are retrieved simultaneously for each transition using a multispectral fitting program.
- The measured collisional half widths, ~0.01 cm^{-1}/atm at 296 K, are about five times smaller than the values listed in the molecular spectroscopy databases.

Graphical Abstract

Graphical Highlight:

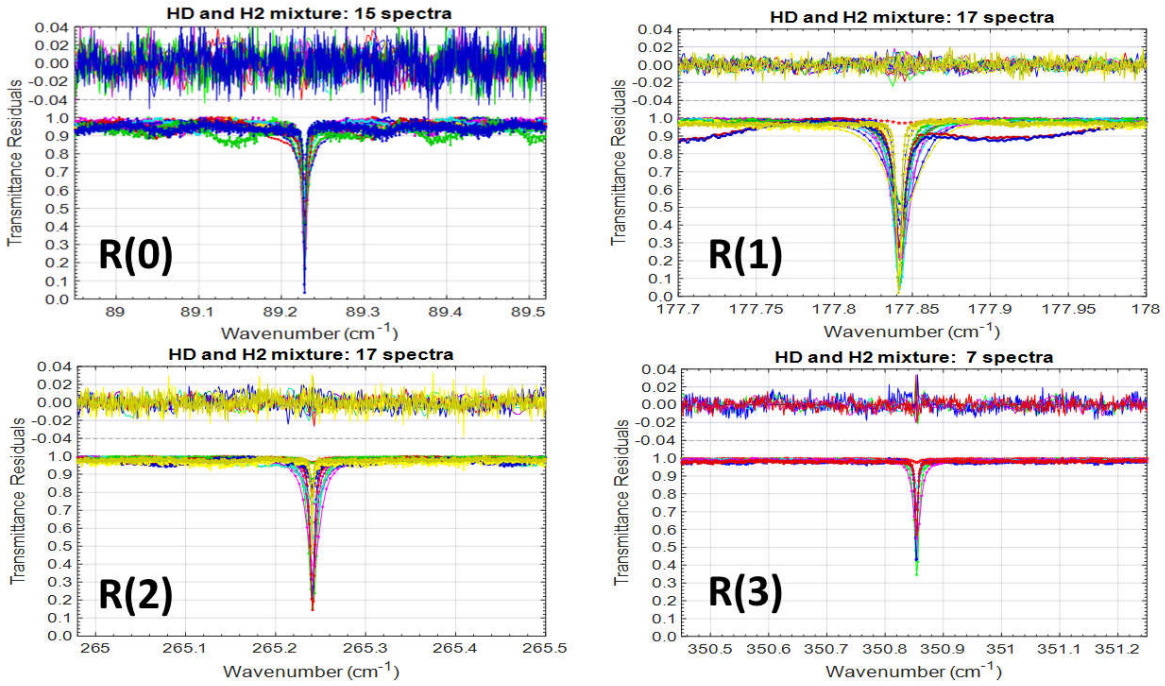

Figure HD and HD-H_2 measured and fitted spectra. The lower part of each panel shows observed (dots) and calculated (solid) spectra. The upper portion shows the fitted residuals (obs-calc). All observed spectra, for each transition, are fit simultaneously such that the residuals are comparable to the measurement noise level.

The rotational spectrum of HD broadened by H_2 at temperatures between 100 – 296 K

Keeyoon Sung[1&], Edward H. Wishnow[2], Brian J. Drouin[1], Laurent Manceron[3], Marine Verseils[3], D. Chris Benner[4], Conor A. Nixon[5]

[1] Jet Propulsion Laboratory, California Institute of Technology, Pasadena, CA, USA.
[2] Space Sciences Laboratory, University of California, Berkeley, CA, 94720, USA.
[3] AILES Beamline, Synchrotron SOLEIL, L'Orme des Merisiers Saint-Aubin, 91192 Gif-sur-Yvette Cedex, France.
[4] Department of Physics, The College of William and Mary, Williamsburg, VA 23187, USA
[5] Planetary Systems Laboratory, NASA Goddard Space Flight Center, Greenbelt, MD 20771, USA.

No. of Tables = 7
No. of Figures = 10

[&] Corresponding author
M/S 200-105, 4800 Oak Grove Dr.
Jet Propulsion Laboratory,
California Institute of Technology
1-818-354-5144
ksung@jpl.nasa.gov

Abstract:

Laboratory measurements of the R(0) – R(3) pure rotational transitions of hydrogen deuteride (HD) have been performed at low pressures (< 1 bar) and temperatures between 98 and 296 K. The measurements were conducted using a Fourier transform spectrometer coupled to the Soleil synchrotron far-infrared source to obtain pure HD and HD-H_2 mixture spectra. The observed spectra have been fitted using a non-linear least-squares multispectral fitting program. For each transition the line position, intensity, pressure broadening, pressure-induced frequency shift, and the temperature dependencies of these quantities have been determined simultaneously. These spectroscopic line parameters are compared to previous measurements made at higher gas pressures. Notably the present, and previous, measurements of the self- and H_2-broadened linewidths are smaller by a factor of five compared with those listed in the HITRAN and GEISA databases. This work is applicable to the low pressure, low temperature regimes found in the atmospheres of the giant gaseous planets.

1 Introduction

The HD molecule, in the vibrational ground state, possesses a small but measurable electric dipole moment, giving rise to angular momentum transitions with selection rules $\Delta J = \pm 1$ first observed in the laboratory in the 1960's [Tre68]. HD is a significant tracer of deuterium in astrophysical contexts, where the deuterium abundance is one of the few observables originating from cosmological nucleosynthesis [Wag67]. The D/H ratio in the gas giant planets can be used to make inferences regarding the formation of the solar system [Bez86; Gri96; Feu99; Lel01; Mou04; Abb10; Feu13] as well as the composition of the primitive solar nebula [Owe92; Léc96]. Cometary D/H ratios vary according to their origins, *e.g.* the Oort cloud as compared to the Kuiper belt [Alt15]. The D/H ratio can be deduced from other molecular species, such as H_2O, CH_4, NH_3 and their D-bearing isotopologues; however, these values are more prone to chemical fractionation effects than the more direct determination from [HD]/[H_2] [dBe86; dBe90; Enc96; Mou04; Abb10].

Accurate determination of HD abundances from observations requires precise knowledge of spectroscopic line parameters, such as positions, intensities, and shape parameters (*e.g.*, collisional broadening, frequency shift coefficients, collisional line narrowing), and their temperature dependences. For example, when HD R(0)–R(2) transition parameters from Feuchtgruber (2013) were used in modelling Cassini/CIRS data of Saturn, the D/H ratio was found to be about 30% lower than on Jupiter [Pie17]; a surprising result that contradicts predictions of a higher value on Saturn, and requires confirmation. The current HITRAN 2020 HD line intensities are calculated values based on a theoretical dipole moment function [Pac08] with uncertainty estimates of 10 – 20 % [Gor22]. Collisional broadening coefficients are generally molecular specific [*See* Var90], and the HITRAN linewidths for HD broadened by H_2 differ substantially (by about a factor of five) from published measurements [Ess84; Dra87a; Dra87b; McK84; McK86; Uli89; Lu93]. There is significant scatter among these measurements, and disagreement with theoretical calculations [SM92]. The HD measured, theoretical and HITRAN transition frequencies, however, all agree to within 0.0001 cm^{-1} [Pac10; Sch87].

Early laboratory measurements were performed at high densities, up to 123 amagat, where collision-induced absorption and collisional interference effects become significant [Tre68; Nel82, Nel83; McK84; Uli89; Uli91; Wis92; Lu93]. Consequently, the measured HD dipole moment showed a variation with density, and these effects have been examined by Poll and co-workers particularly [Pol76; Tip78; Ma85; Pol85; also Tab85]. The permanent dipole moment, exclusive of interference effects, is however, independent of density, and in the vibrational ground state it is theoretically expected to vary only slightly with rotational state [Pac08; Joz20].

The present study is an effort to measure the HD spectrum using experimental conditions close to those of planetary atmospheres. Spectra have been obtained over the 50 – 360 cm^{-1} range, at very high spectral resolution, and the data analyzed using a multispectrum fitting program to determine spectroscopic line parameters for the R(0) – R(3) transitions. A collisional (Dicke) narrowing effect was observed in laboratory spectra [Ess84], so a non-Voigt line shape profile has been used in the fitting.

2 Experimental details

2.1 Interferometer and gas cells

HD rotational transitions weakly absorb radiation, and measurements of low pressure samples require fairly long absorption paths. Furthermore, the Doppler width at low temperature in the far-infrared is very small, and pure HD measurements at low pressures require operating the spectrometer at its highest resolution. The use of the synchrotron radiation source permitted measurements of the R(0)-R(3) rotational transitions at high spectral resolution (~0.0006 cm^{-1}), with good signal-to-noise, over a reasonable experimental time period.

Measurements were conducted on the AILES beamline at the Synchrotron Soleil, France, during two sessions: 2018 Nov 10-17, and 2019 Sep 23-27. The far-infrared source was coupled to a Bruker 125HR Fourier transform spectrometer, and the radiation then passed through a Chernin-type low-temperature multipass absorption cell to a bolometer detector, as described in Tchana et al [Tch13]. The entire beam path, exclusive of the absorption cell, was evacuated. The spectral resolution of the measurements was tailored to the density of the gas sample, and the highest resolution employed was 0.00056 cm^{-1} (0.5/L, where L is the maximum optical path difference, Bruker res. = 0.00102 cm^{-1}). The temperature of the gas sample was determined from an average of selected platinum resistors placed at different locations inside the cell or attached to the inner cell wall surface. The cell was cooled with liquid N_2, where the temperature was controlled by changing the pressure of a helium exchange gas in a chamber surrounding the cell, and by electrical heaters attached to the cell. Once a stable condition was established, the average temperature varied only by about ±1.5 K over a week. This spectrometer system was previously used in a study of NH_3 with the same multipass cell at room temperature [Yu10; Sun16]. Measurements were made using three different absorption pathlengths chosen to achieve measurable peak absorptions and to avoid saturation.

A second straight-through cell, 5.1 cm long, was used for pure HD measurements at higher pressures. The short cell was also completely enclosed by the vacuum system. This cell was used at cold and room temperatures, and it was cooled by flowing cold N_2 gas through coils attached to its exterior. The experimental conditions are listed in Table 1 below.

Table 1. Experimental Parameters and Conditions

Spectral Region	50 – 360 cm^{-1}
IR source	AILES beamline, Synchrotron Soleil
Beam Splitter	6 µm Ge on Mylar
Scan rate (HeNe fringes)	60 KHz
Detector	4 K Bolometer + 400 cm^{-1} lowpass filter
Spectral resolutions	up to 0.00056 cm^{-1} (unapodized) [Bruker res. 0.00102 cm^{-1}]
Gas samples	HD (98.73%) and H_2 (≥ 99.99%)
Absorption path lengths (m)	0.051, 3.14, 9.14, 21.14
Gas cell windows	Diamond, 0.4 mm thick
Sample temperatures	98 – 296 K
Sample pressures (mb)[a]	20 – 1002 for HD; 100 – 1002 for HD+H_2 mixtures
Temp. sensors (accuracy 0.1 K)	Platinum resistance thermometers, various cell locations
Frequency calibration standards	H_2O in the 200 cm^{-1} region[b]

[a] 1 atm = 760 Torr = 1013 mb.;
[b] Features from residual water in the FT-IR chamber (*i.e.,* not from the sample cell).

2.3 Sample Conditions and Experimental Procedures

The gas sample pressures were monitored by a set of capacitance gauges during the entire data collection period. The high purity HD was purchased from Cambridge Isotope, Inc. (Euristop). The certified purity was HD (98.73%), H_2 (0.76%), and D_2 (0.51%). The H_2 broadening gas was research grade purity (99.99%) and the extra HD impurity in the H_2 sample was taken into account using the natural abundance values listed in HITRAN 2020 [Gor22] (*e.g.,* H_2 0.999668 and HD 0.000311432). The partial pressures of HD and H_2 in a mixture are computed from the pressure readings of HD (P_{HD}) and H_2 (P_{H2}), by:

$$\text{Total HD} = 0.9873 \times P_{HD} + 0.0003114 \times P_{H2} \qquad \text{(Eq.1a)}$$

$$\text{Total } H_2 = 0.0076 \times P_{HD} + 0.999688 \times P_{H2} \qquad \text{(Eq.1b)}$$

The data acquisition procedure began by cooling the multipass cell. Once a stable cell temperature was achieved, an initial sample of pure HD was admitted to the cell and very high resolution spectra were obtained. Nearly 24 hours of interferometer scans were collected to achieve adequate signal-to-noise for these highest resolution measurements. H_2 broadening gas was then added to the HD sample to obtain a mixture spectrum which, due to the higher pressure, can be resolved at lower spectral resolution. The process of adding H_2 to the mixture continued, and spectra of various mixing ratios were obtained. Sets of corresponding background spectra were obtained at the lower

resolution with an empty cell or H_2 at a comparable pressure to the sample gas (at these low pressures the collision-induced absorption of H_2 is unmeasurable). For the case of short cell measurements at room temperature, N_2 gas was used for the background. In many cases the empty cell spectra had a continuum level that was more consistent with the sample spectra. In total, three pure HD spectra and 14 HD+H_2 mixture spectra were acquired between 98 and 297 K, and the experimental conditions are summarized in Table 2.

Table 2. Measurement conditions for HD & HD-H2 spectra

Spec No.	P_s (mb)	P_t (mb)	L (m)	T (K)	Res(B) (cm^{-1})[&]	R0123[#]
3 spectra of Pure HD spectra						
1	1002.3	1002.3	0.051	298.0(1)	0.01	- 1 2 3
2	988.0	988.0	0.051	176.0(10)	0.01	- 1 2 -
3	35.2	35.2	3.14	95.4(10)	0.00102	0 1 2 -
14 spectra of HD + H_2 mixture						
4	46.5	151.8	9.14	295.8(8)	0.002	0 1 2 3
5	46.5	300.8	21.14	296.0(8)	0.004	0 1 2 3
6	46.5	624.8	21.14	295.7(8)	0.009	0 1 2 3
7	20.2	601.0*	21.14	193.3(1)	0.009	0 1 2 3
8	20.2	300.0*	21.14	193.1(7)	0.002	0 1 2 3
9	20.2	151.5*	21.14	192.4(4)	0.002	0 1 2 3
10	35.2	910.3	9.14	129.7(9)	0.01	0 1 2 -
11	35.6	921.9	9.14	128.6(13)	0.02	0 1 2 -
12	35.2	415.5	9.14	123.5(16)	0.005	0 1 2 -
13	34.2	206.0	9.14	118.5(4)	0.005	0 1 2 -
14	35.2	201.0	3.14	101.2(6)	0.003	0 1 2 -
15	35.2	300.0	3.14	100.3(5)	0.003	0 1 2 -
16	35.2	400.0	3.14	100.1(3)	0.005	0 1 2 -
17	35.1	106.5	3.14	98.1(9)	0.0017	0 1 2 -

Notes: P_t = Total pressure (*i.e.* HD + H_2); P_s = HD sample pressure
[&] Res(B) = Bruker FTS resolution parameter.
*A 1 mb of CO was added to test the instrumental line shape and the spectral line resolving power for the given spectral resolutions. The presence of the CO did not impact the HD line parameter retrieval.
[#] Fitted HD transitions for which parameters are retrieved.

Transmission spectra are formed by dividing sample spectra by the best consistent set among the background spectra. For example, transmission spectra are selected from those that produce the least prominent 'channel' spectra (unavoidable ripples that arise from subtle differences between sample and background spectra). The signal-to-noise of the transmission spectra formed is ~100, depending on the spectral region and resolution. An example of a HD-H_2 transmission spectrum at 192 K is shown in Fig 1, where all four HD lines have measurable intensity, and the R(0) – R(3) transitions are seen near 89.23, 177.84, 265.24, and 350.85 cm^{-1}, respectively.

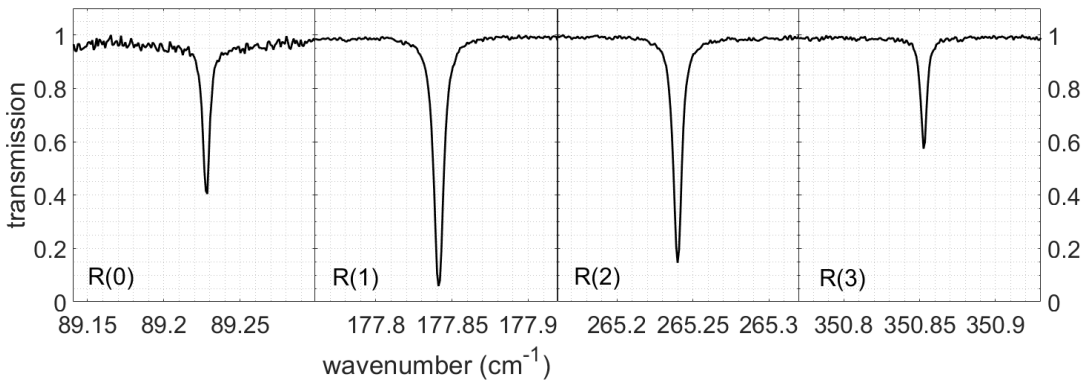

Fig. 1 The R(0) – R(3) transitions of the HD-H_2 transmission spectrum at 192 K over an optical path of 21.14 m. The HD pressure is 20.2 mb and the total sample pressure is 151.5 mb.

3 Data analysis

3.1 Frequency calibration

All the HD spectra have been frequency calibrated using a few well-isolated H_2O lines. These features arise from residual water vapor in the evacuated FTS chamber, which is at room temperature. Since the pressure of the FTS chamber is very low, the water lines are quite narrow with no significant pressure shift. H_2O is not present in the cold gas samples as it condenses in the cell fill tube or on the walls. The spectra at room temperature exhibit, however, pressure broadened H_2O contaminant features with the superposed sharp lines from the FTS chamber. The frequencies of the sharp components of the H_2O lines are compared to those listed in HITRAN 2020 [Gor22] to obtain a calibration factor. The calibrated spectra have a frequency accuracy of better than 0.0001 cm^{-1}.

3.2 Retrievals through multispectrum fitting analysis

For each HD transition, all the pure HD and HD-H_2 mixture spectra with measureable absorption were fitted simultaneously; spectra included in the fit are indicated in the last column in Table 1. The spectroscopic parameters shown in Table 4 were thereby obtained using the Labfit multispectrum fitting software package [Ben95; Let07; Dro17], which is based on an iterative nonlinear least squares curve fitting algorithm. The package uses a non-Voigt spectral line shape. This analysis technique has produced high quality results for various molecules [Dev10; Dev16a; Dev16b; Sun20].

Mathematical details of the multispectrum fitting package have been presented previously [Sun20], and a brief summary of it is presented below. For a transition centered at ν_0, the cross section $k(\nu - \nu_0)$ can be written as

$$k(\nu - \nu_0) = S \cdot \kappa(\nu - \nu_0) \qquad \text{(Eq. 2)}$$

where S is the line intensity and κ is the molecular line shape profile. A non-Voigt profile, $\psi(x, y, \epsilon)$, is used which is defined in terms of the complementary complex probability function, $W(z)$, [Hum82] and unitless parameters, $z = x + i(y + \epsilon)$, $x = \sqrt{\ln(2)}\,(\nu - \nu_0)/\gamma_D$, $y = \sqrt{\ln(2)}\,\gamma_L/\gamma_D$, $\epsilon = \sqrt{\ln(2)}\,\beta/\gamma_D$, where ν_0 is the line center frequency in vacuum, γ_D is the Doppler half-width, γ_L is the pressure-broadened half-width, and β is the collisional narrowing parameter, respectively. The present analysis uses the hard-collision model with the Rautian line profile [Rau67; Pin92; Ben95]. Thus, Eq.(2) can be expanded to:

$$W(z) = \left(\frac{i}{\pi}\right) \int \exp(-t^2)\,(z - t)\,dt \qquad \text{(Eq. 3a)}$$

$$\kappa(\nu - \nu_0) = \psi(x, y, \epsilon) = Re\left[\frac{W(z)}{1 - \sqrt{\pi}\,\epsilon\,W(z)}\right] \qquad \text{(Eq. 3b)}$$

where $z = x + i(y + \epsilon)$. The Lorentz half-width, γ_L, and the line position, ν_0, as a function of pressure (P) and temperature (T), are based on an empirical model with the line position in vacuum, ν_{00}, and the coefficients, γ^o, δ_0, and δ' described in Table 3 [Ben16; Dev16a; Dev16b]:

$$\gamma_L(P, T) = P \times [\gamma^0(T_0) \times \left(\frac{T_0}{T}\right)^n] \qquad \text{(Eq. 4)}$$

$$\nu_0(P, T) = \nu_{00} + P \times [\delta^0(T_0) + \delta' \times (T - T_0)]. \qquad \text{(Eq. 5)}$$

Table 3 Spectroscopic line parameters for each transition

symbols	full description	Units	Short names
ν_0	zero pressure line center position	cm^{-1}	position
S	line intensity at 296 K	cm^{-1}/ (molecule·cm^{-2})	intensity
γ^0	(HD or H_2) pressure-broadened half-width coefficient at 296 K at 1 atm (*See* Eq. 4)	cm^{-1}/atm	self-width; H_2-width
n	temperature dependence exponent of the half-width coefficient (*See* Eq. 4)	unitless	width T-dep.
δ^0	(HD or H_2) pressure-induced line shift coefficient at 296 K at 1 atm (*See* Eq. 5)	cm^{-1}/atm	self-shift; H_2-shift
δ'	temperature dependence parameter of the pressure-shift coefficient (*See* Eq. 5)	cm^{-1}/(atm·K)	shift T-dep.
β	Collisional narrowing parameter (*See* Eq. 3b)	cm^{-1}/atm	narrowing

The lowest pressure and temperature far-infrared spectral linewidths are Doppler limited and the pure HD spectra were just resolved (excepting R(0)) using the highest spectral resolution possible with the FTS. The synchrotron radiation source is understood to have a frequency dependent

effective beam diameter [Jaq10], with an effective value, d_{eff}, modeled by Eq. (6) [Man19]; this divergence apodization effect on the spectral resolution is included in the fitting process.

$$d_{eff}(mm) \approx \frac{25}{\sqrt{\nu}}, \text{ where } \nu \text{ is wavenumber in cm}^{-1}. \quad \text{(Eq. 6)}$$

Each HD transition was treated separately, but applicable spectra at various temperature and pressure conditions were fitted simultaneously (see Table 2). The transitions were treated independently since, for instance R(0) and R(3) lines were too weak at either room temperature or low temperature, respectively. Since the number of pure HD spectra is limited, the temperature dependence of the self-broadening coefficient, n, has been constrained to that of the HD-H_2 broadening. The multispectrum fitting procedure adjusts the spectroscopic line parameters until the differences between the observed and synthetic spectra converge to a minimum, typically at the measurement noise level. A set of continuum oscillations that accounts for 'channel spectra' is also included in the fitting process. The fitted spectra, and residuals, of the four transitions are shown in Fig. 2, and the number of spectra used in the fits is shown above each panel.

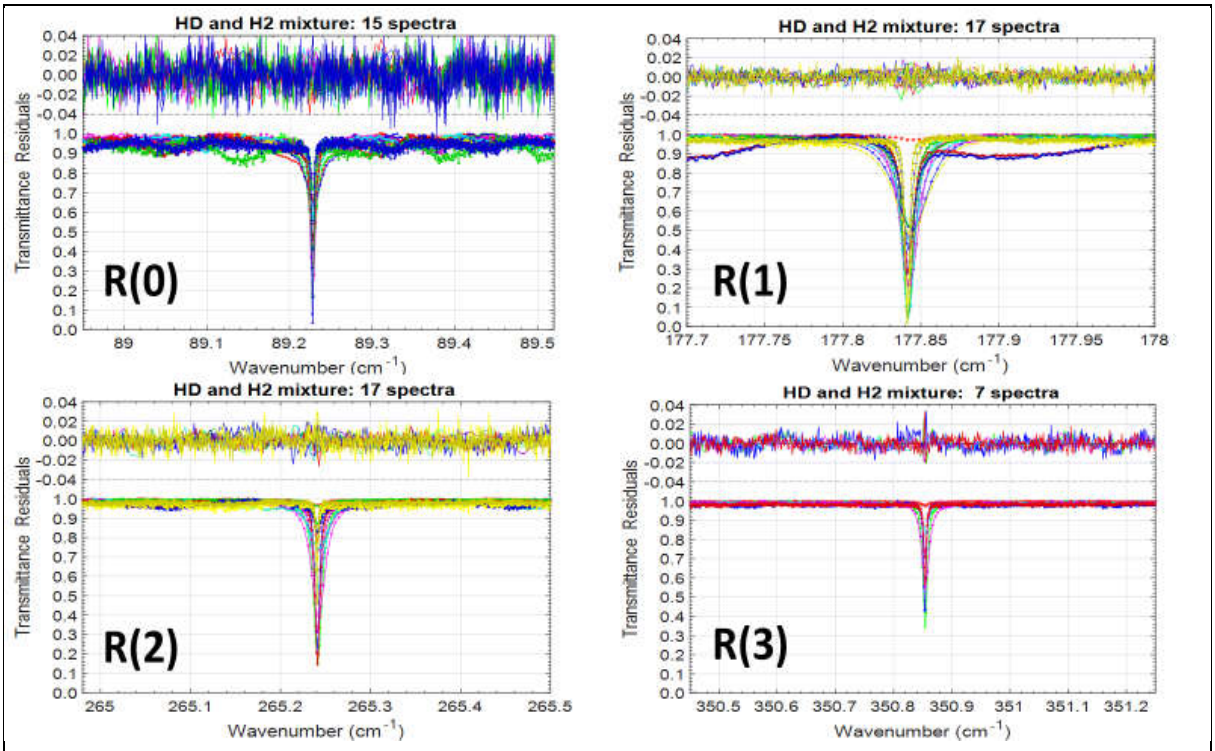

Fig. 2 HD and HD-H_2 mixture spectra, measured and fitted. The lower part of each panel shows observed (dots) and calculated (solid) spectra. The upper portion shows their fitted residuals (*Obs-Calc*). For each transition, all spectra are fit simultaneously such that the residuals are comparable to the measurement noise level.

4. Results and Comparison

4.1 Overview of the HD line parameter retrievals

The spectroscopic line parameters derived from the fitting of the HD and HD-H_2 measurements are shown in Table 4. Comparisons are made to previous measurements and the latest version of the HITRAN 2020 database [Gor22; http://www.hitran.org] in the following sections.

Table 4 HD line parameters and uncertainties retrieved from fitted spectra.

Transitions Parameters@296K	R(0)	R(1)	R(2)	R(3)
ν_0, Position (cm^{-1})	89.22792(3)	177.84141(3)	265.24055(3)	350.85401(4)
S intensity (cm/molecule)	$5.561(36)\times10^{-28}$	$2.402(5)\times10^{-27}$	$2.886(9)\times10^{-27}$	$1.522(7)\times10^{-27}$
γ^0 H_2-width (cm^{-1}/atm)	0.0120(4)	0.0114(1)	0.0104(1)	0.0097(2)
γ^0 self-width (cm^{-1}/atm)	0.0114(7)	0.0125(2)	0.0131(5)	0.0081(7)
n H_2-width expon. (no unit)	-0.027(37)	0.127(10)	0.174(13)	0.141(40)
n self-width expon. (no unit)	-0.027(37)[c]	0.127(10)[c]	0.174(13)[c]	0.165(40)[c]
δ^0 H_2-shift (cm^{-1}/atm)	0.00017(35)	0.00141(22)	0.00106(13)	-0.00108(17)
δ^0 self-shift (cm^{-1}/atm)	0.00017(35)[c]	0.00518(68)	0.00633(89)	-0.00108(17)[c]
δ' H_2-shift (cm^{-1}/atm/K)	-0.000007(2)	-0.000010(1)	-0.000006(1)	-0.000011(2)
δ' self-shift (cm^{-1}/atm/K)	-0.000007(2)[c]	0.000015(4)	0.000022(5)	-0.000011(2)[c]
β, narrowing (cm^{-1}/atm)	n/a	0.017(10)	0.033(15)	n/a

Notes:
[1] Position, intensity, half-widths, shifts, narrowing parameters are the values at T_0 = 296 K.
[2] Line intensity includes the natural abundance following the HITRAN convention.
[3] Self-parameters flagged with 'c' are constrained to their corresponding H_2-parameters due to a limited number of pure sample spectra.

The uncertainties shown in Table 4 are the errors that result from the multispectrum fitting process. As shown in Fig. 2, all the four HD transitions are very well modelled down to their spectral noise levels. Their peak-to-peak signal-to-noise (S/N) values are 73, 188, 159, 180, respectively, and the retrieval errors are due to these limitations. The systematic errors of the experiment, which exceed the fitting errors, are discussed in Sec. 5.

4.2 Transition frequencies

Table 5. Comparison of line center positions of HD

Position (cm^{-1})	R(0)	R(1)	R(2)	R(3)
HITRAN 2020	89.2279(1)	177.8413(1)	265.2401(1)	350.8530(1)
Measurements[&]				
This work	89.2279(1)	177.8414(1)	265.2406(1)	350.8540(1)
JPL Catalog	89.22793(0)	177.84127(2)		
Drouin 2011	89.2279316(8)			
Ulivi 1991		177.84172(16)	265.24116(17)	350.85295(12)
Evenson 1988	89.227950(5)			
McKellar 1986		177.828(2)	265.207(2)	350.844(2)
E&G 1984				350.852(2)
Theoretical calculations				
Wolniewicz 1983*	89.228	177.841	265.239	350.852
Ulivi 1991	89.227950(5)	177.841790(17)	265.241119(55)	350.85295(11)
P&K 2010	89.227933(8)			
Jozwiak 2020[#]	89.2279(2)	177.84127	265.24009	350.85301
Czachorowski 2018*	89.226758	177.83894	265.23666	350.84854

[&] References for the measurements are JPL Catalog [Pic91; http://spec.jpl.nasa.gov], Drouin2011 [Dro11], Ulivi 1991 [Uli91], Evenson 1988 [Evn88], McKellar 1986 [McK86], E&G [Ess84], Wolniewicz 1983[Wol83], P&K 2010[Pac10], Jozwiak 2020 [Joz20], Czachorowski 2018 [Cza18].
[#] Calculated with H2Spectre code of Czachorowski et al. [Cza18] and [Kom19] .
* Obtained from differences in the dissociation energy table.

Retrieved spectral transition frequencies are listed in Table 5 and compared to previous measurements and theoretical predictions in Fig. 3. Figure 3 shows transition frequency differences compared to the HITRAN 2020 values after sorting them by publication year along the x-axis. The HITRAN values and the present work are denoted by square and circle symbols, respectively, throughout this paper. For the R(0) transition, the present value agrees well with the high resolution value measured at 18 K reported by Drouin et al. [Dro11], and it also corresponds to the latest theoretical calculations which have been adopted by HITRAN [Joz20].

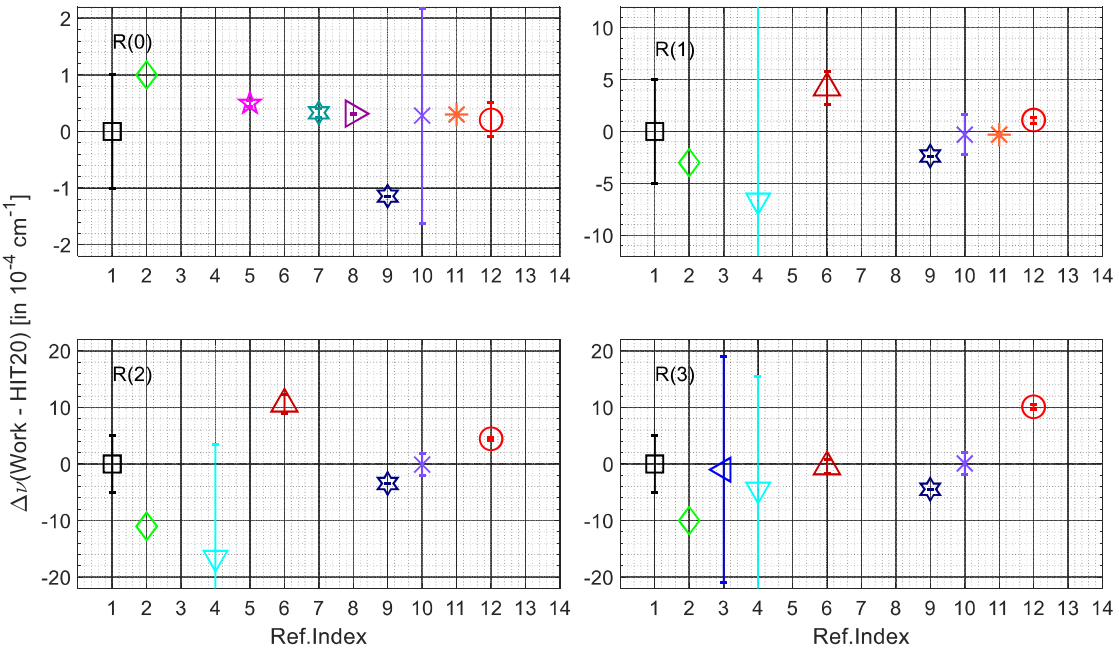

Fig. 3 Line position differences (in cm^{-1}) compared to HITRAN for previous measurements and theory. The reference indices and symbols are: 1: HITRAN 2020(□), 2: Wol83(◊), 3: EG84(◁), 4: McK86(▽), 5: Evn88(☆), 6: Uli91(△), 7: Pac10(Hexagram), 8: Dro11(▷), 9: Cza18(Hexagram), 10: Joz20(x), 11: JPL Catalog(*), 12: This work(○). Note that the y-axis range for R(0) and R(1) are smaller than the other two. The deviations of E&G84(◁) and Mc86(▽) have been divided by factors of 10 and 20, respectively.

In general, all the R(0) values are comparable to HITRAN. The R(1) transition is reasonably absorptive for all temperatures studied in the present work. Its position was retrieved with the lowest uncertainty and it agrees with HITRAN to within 0.0001 cm^{-1}, *i.e.* the accuracy of the frequency calibration of this work. The R(1) measurement by Ulivi et al. [Uli91] and the calculation by Wolniewicz [Wol83] are within 0.0003 cm^{-1}, although their studies are more than three decades old. The R(2) transition also has adequate optical density at all measured temperatures, and it has a low uncertainty similar to that for R(1). The R(2) value determined herein is 0.0005 cm^{-1} higher than HITRAN, but it is lower than the Ulivi et al. [Uli91] measurements by ~0.0005 cm^{-1}. The population of the J = 3 state is low at cold temperatures, and only seven spectra were used in the fitting; thus, the uncertainly of the R(3) position is larger than that of R(1) and R(2). The R(3) result is larger than the HITRAN value by 0.0010 cm^{-1}, and larger than that of Ulivi et al.[Uli91] by a similar amount. There is a correspondence, however, within probable errors with a previous diode laser measurement of Essenwanger and Gush [E&G84].

4.3 HD line intensities and dipole moments

A goal of the present work is to determine HD and HD-H_2 spectroscopic line parameters in a form that will be useful to modelers of planetary atmospheres. The line intensity S, which is temperature and rotational state dependent, has been obtained through the multispectrum fitting process in the HITRAN formulation at the reference temperature 296 K [Rot98]. The physical property of the molecular dipole moment is, however, temperature independent and its determination has been an objective of previous experimental and theoretical studies [Wol76, Nel83, Ess84; McK84; McK86; Dra87a; Dra87b; Uli91; Wis92; Lu93; Pac08; Joc20]. The relationship between the line intensity S and the molecular dipole moment μ is given by:

$$S_{JJ'}(T) = \left(\frac{8\pi^3}{3hc}\right)\nu_{JJ'}\frac{I_a g_{spin}}{Q(T)}\exp\left(-\frac{c_2 E_J}{T}\right)\left[1-\exp\left(-\frac{c_2\nu_{JJ'}}{T}\right)\right]\times\mu^2(J+1) \quad \text{(Eq. 7)}$$

where the details of this equation are given in the Appendix.

The new dipole moment results are compared to previous work and the HITRAN values in Fig. 4. The four transitions are shown in separate panels with HITRAN values denoted as open squares and the present results as open circles throughout this manuscript, with both having solid horizontal lines color-coded for comparison purposes. The previous values are sorted by their references. Figure 4 shows that the present results are slightly smaller than the HITRAN values for all transitions. For the transitions R(0), R(2), and R(3) the present results are comparable to an average of previous experimental results; for R(1) the present value is a little higher than an average of the experiments and rather closer to the theoretical value.

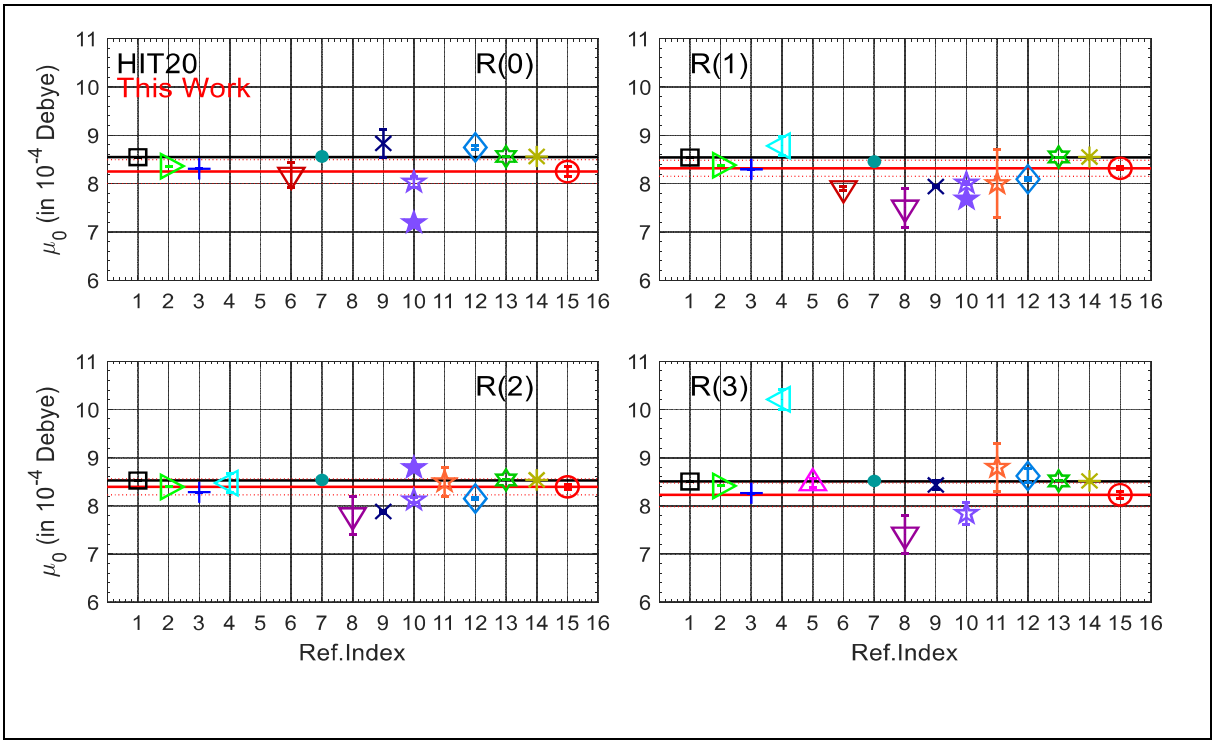

Fig. 4. Comparison of HD molecular dipole moment measurements and theory. The reference indices and symbols are 1: HITRAN(□), 2: Wol76(▷), 3: For77(+), 4: Nel83(◁), 5: Ess84(△), 6: McK84(▽), 7: Tho85(●), 8: McK86(▽), 9: Dra87(x), 10: Uli89(☆), 11: Uli91(☆), 12: Lu93(◊), 13: Pac08(hexagram), 14: Joz20(*), 15: This work(○). Multiple data points for the same source indicates that measurements were made at more than one temperature. Missing symbols for some references indicates that their values are outside the plotted regions.

Figure 5a shows a comparison between the newly derived line intensities, *S*, and previous measurements at various temperatures. For HITRAN and the newly retrieved line intensities at 296 K, the intensity values at all other temperatures are computed using Eq. A11 of Rothman et al. [Rot98]; these extrapolations are shown as continuous lines. Previous experimental dipole moment values at particular temperatures are likewise converted to a line intensity, *S*, using Eq. 7 above, and these data are shown as individual points. The lower panels of Fig. 5b show percentage differences between the extrapolated HITRAN and other measurements in order to accentuate the variations. Here the present measurements are depicted by open circles at three specific temperatures. The HITRAN values are adopted from theoretical calculations, which have an uncertainty of 10 – 20% [Pac08], and this is shown by the dashed lines in red in the figure. The present results fall within ~5% of these theoretical values for all transitions and temperatures.

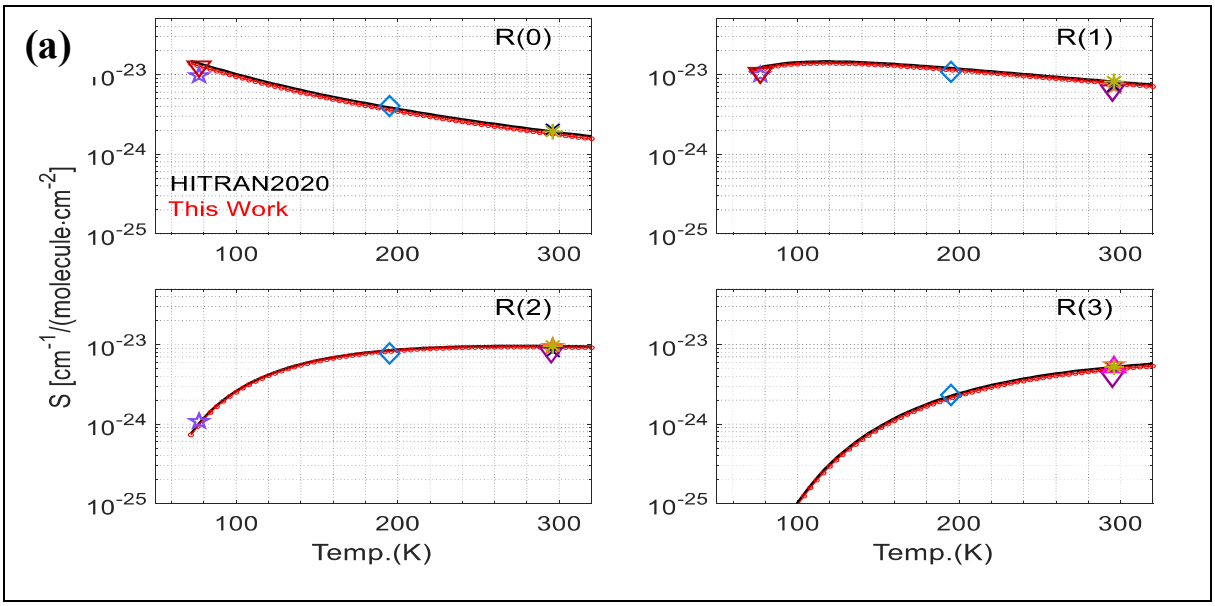

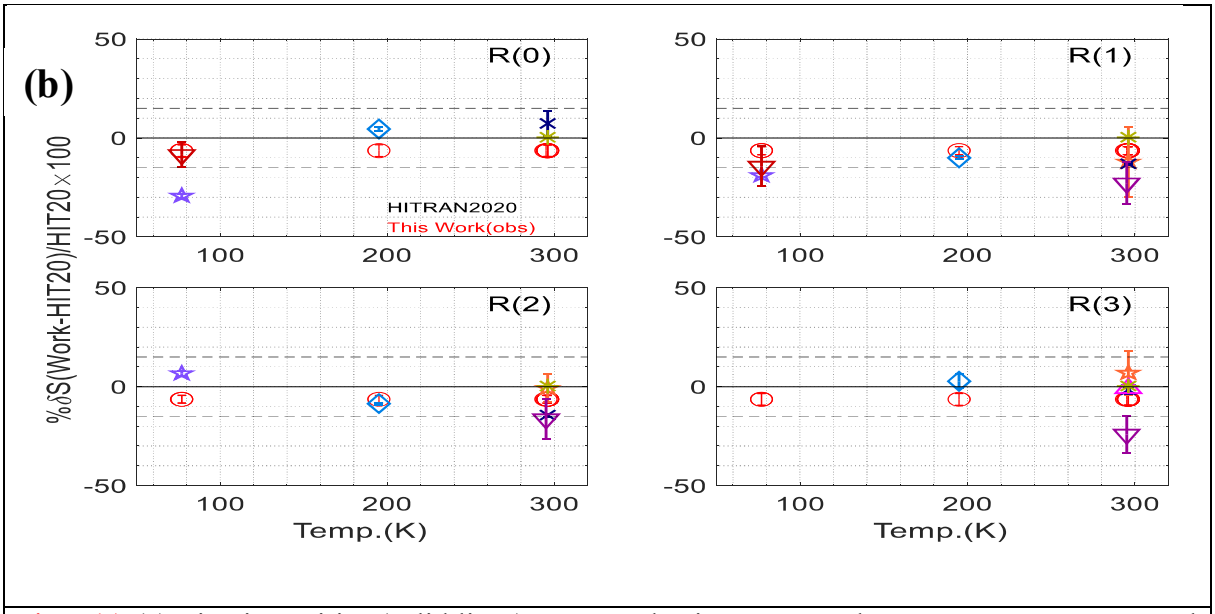

Fig. 5(a) (a) Line intensities (solid lines) computed using Eq. 7 and HITRAN parameters, and fitted parameters in Table 4, are compared with previous measurements (symbols) (b) The differences between line intensities of HITRAN 2020 and previous experiments at various temperatures: Ess84(△), McK84(▽), McK86 (▽), Dra87(x), Uli89(☆), Uli91(☆), Lu93(◊), Joz20(*), and this work (○). Intensities derived from the present work are shown at the discrete temperatures of previous experiments.

Since the HD dipole moment is quite small, collision-induced absorption, and collisional interference effects can be pronounced compared to the allowed dipole moment transitions [Pol85]. Measurements of the fundamental band show large line asymmetries with increasing gas densities, and these lines are well fitted by a Fano line shape (e.g. Rich & McKellar [Ric83]). The line asymmetries are significantly less prominent in the rotational band even at relatively large gas densities. The rotational band experiments of McKellar et al. [McK84, McK86], and Tabisz et al. [Uli89, Uli91, Lu93] were also fitted with Fano line shapes although the asymmetries are quite small and the density dependent interference parameters are of order 10^{-3}/amagat. The molecular dipole moment in these previous experiments is obtained by extrapolating the integrated line intensity to zero density.

The present experiments were conducted using temperatures and densities closer to those of giant planet atmospheres [Nix09; Nix20]. Gas densities used were below 2.0 amagat and collisional effects contribute less than a fraction of 1% to the line intensity. Using low gas densities permitted the fitting of the spectra with a symmetric line shape and a density-independent intensity parameter (see Table 3). The fits shown in Fig. 2 show no residual asymmetry above the experimental noise level. The measured dipole moment is nearly constant as a function of rotational state, and within experimental error this corresponds to theoretical predictions for the pure rotational band [Joz20]. Collisional narrowing is considered as part of the fitted line shape and it is discussed below.

4.4 HD line shape parameters – width, shifts, and narrowing

4.4.1 Pressure-broadening of the HD transitions

The HD self-broadening and H_2-broadening coefficients, γ^0 (cm^{-1}/atm) at 296 K, are retrieved simultaneously and independently through the multispectrum fitting process. Despite a limited number of pure HD spectra, the fitting process also retrieves self-broadening parameters by using the HD partial pressures in the multiple sets of the HD-H_2 mixtures. The temperature dependence parameter (n in Eq. 4) for H_2-broadening is also retrieved for each transition. The self-broadening temperature dependence, however, is constrained to that of H_2-broadening due to the limited number of pure HD spectra.

Comparisons of the present broadening parameters and their variations with temperature to previous work are shown for the self-broadened half-widths in Fig. 6a, and for the H_2-broadened half-widths in Fig. 6b. In these figures measurements of full width at half maximum (FWHM), B_0 in cm^{-1}/amagat, reported by earlier work [Ess84; McK84, McK86; Dra87; Uli89; Lu93] have been converted to HITRAN units, cm^{-1}/atm, HWHM to facilitate comparisons. Note that the temperature dependence for the half-width, γ (cm^{-1}/atm), in Eq. 4 can also be applied to the full width, B_0 (cm^{-1}/amagat), as long as their units are kept consistent with those of Eq. 4. HITRAN [Gor22] and Feuchtgruber et al. [Feu13] provide temperature dependence parameters based on Eq. 4 referenced to $T_0 = 296$K, and Lu et al. [Lu93] provides parameters referenced to $T_0 = 77$ K. These results are plotted continuously over the temperature range in Fig.6. Feuchtgruber et al. [Feu13] is not an experimental result, but a critical compilation of existing measurements (based on [Evn88; Uli91; Lu93]) for a perturbing gas composed of a H_2: He [85:15] mixture. The most prominent finding is that the collisional broadening values listed in HITRAN 2020 are larger than the experimental measurements by about a factor of 5; to place the HITRAN values on the comparison figure they have been multiplied by 0.2. The HITRAN temperature dependent exponent also does not fit the low temperature measurements. The plot of H_2 broadening of the R(0) line includes theoretical values of Schaefer and Monchick [SM92]; these data are generated using their Table 6 and their Eq. 18, after including the implicit parameter, L_0, Loschmidt's number ($2.689\times10^{19}/cm^3$).

Inspection of Figs. 6a and 6b shows that our new measurements (in open red circles) are generally consistent with previous experimental results, particularly at the lowest temperatures. The new results differ substantially from the rescaled HITRAN values. The H_2-broadening (Fig. 6b) shows somewhat a closer correspondence to previous measurements than the self-broadening (Fig. 6a). The major discrepancy is that current measurements of the self-broadening of the R(2) transition differ substantially from previous measurements.

Theoretical calculations by Shaefer and Monchick [SM92] show that H_2-broadening of the R(0) transition has a minimum near 80 K, where there is fairly good agreement with our measurements. Their calculations differ, however, from the present and previous measurements at temperatures higher than 140 K [Lu93]. In these figures it is apparent that the HITRAN temperature exponents do not match well the experimental values. The present results are a closer match, but some discrepancies remain due perhaps to adopting a simple model for the temperature dependence of the linewidth (*See* Eq. 4). Since the new results have been derived from simultaneously fitting

spectra over all temperatures and pressures, they are expected to have good consistency among the retrieved parameters.

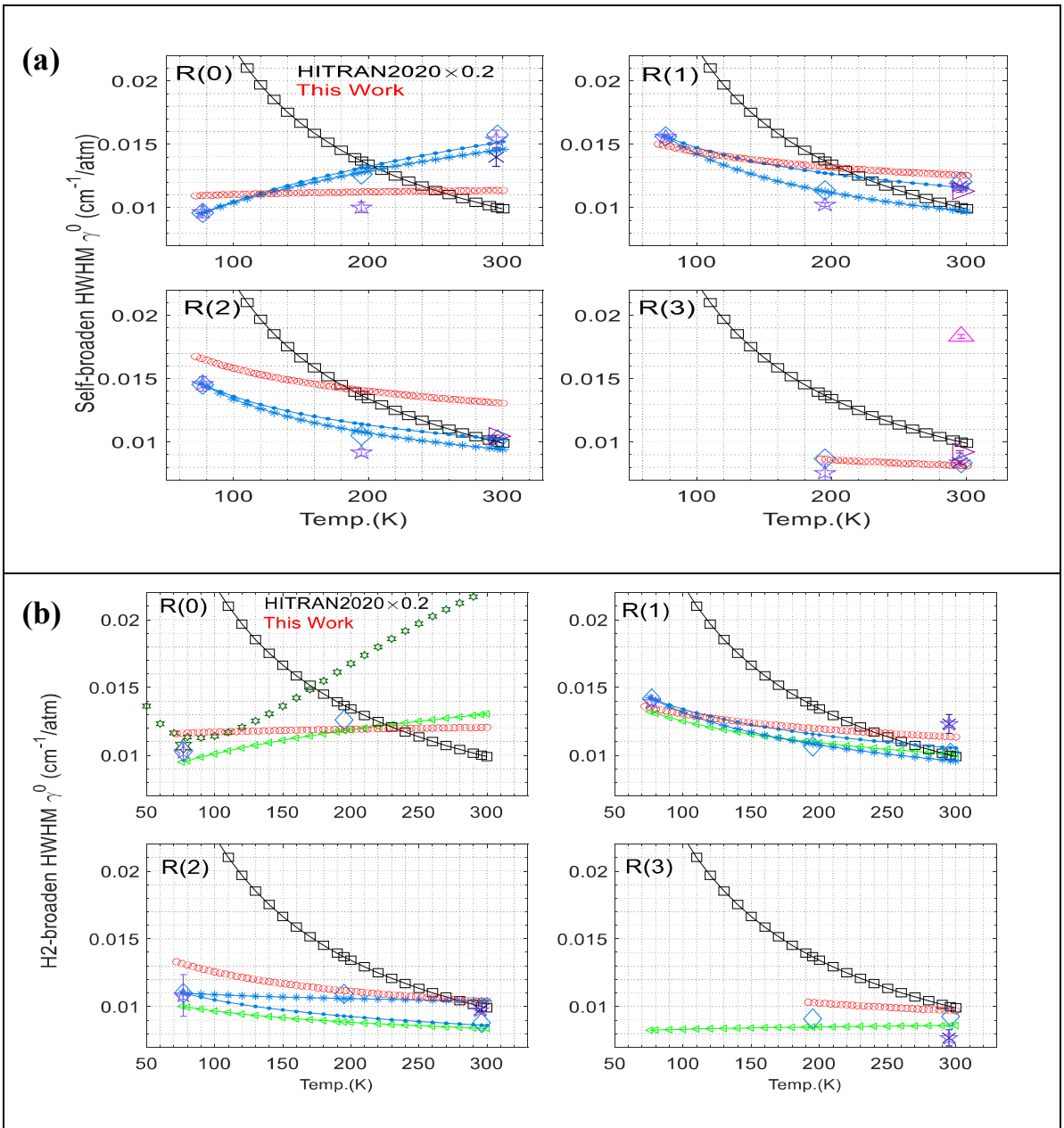

Fig. 6 Comparison of (a) Self- and (b) H_2-pressure-broadened line widths, HWHM (in cm^{-1}/atm). The symbols are for HITRAN 2020 (□), Feu13(◁), Ess84 (△), McK84 (▽), McK86(▷), Dra87(x), Uli89(☆), Lu93(◊), SM92 (hexagram), and this work (○).The series of symbols, Lu93 (*) and Lu93 (●), presented across the temperature ranges are extrapolations using the empirical model, Eq. 4, based on measurements at 77, 195 and 296 K, respectively, with T_{ref} = 77 K. The present data series are calculated using Eq.4 and the fitted parameters of Table 4. Note that the HITRAN 2020 widths are reduced by a factor of 5.

4.4.2 Pressure-induced frequency shifts

Pressure-induced frequency shifts and temperature dependencies, δ^0 (cm^{-1}/atm), for the R(0)–R(3) transitions have been retrieved from the fit. There was adequate data to obtain both HD self-shifts and H_2 induced shifts for R(1) and R(2), but the self-shifts and temperature dependent exponents of R(0) and R(3) have been constrained to the values of the H_2-induced shifts for these two lines. The self- shift values have not previously been listed in the HITRAN [Gor22] or GEISA [Jac16] databases. The self and H_2 frequency shift results, extrapolated over the temperature range 77 – 300 K, are shown in Figs. 7a and 7b, respectively. The present work is shown as the continuous string of open circles. Previous measurements at discrete temperatures, again converted to HITRAN units, are also plotted for comparison. The shift values for all transitions over all temperatures are quite small. The agreement between the current work and previous measurements is better for the H_2 frequency shifts than those for the self-shift cases, and the current work matches reasonably well the previous R(0) – R(2) H_2 values.

The situation for R(0) is particularly interesting as the present results show a *positive* frequency shift with pressure at for all measured temperatures, but previous precise measurements by Drouin et al. [Dro11] at 18 K show a clear *negative* shift. Schafer and Monchick [SM92] conducted a theoretical study of H_2-shifts for R(0), which indeed shows a change in the sign of the frequency shift with temperature. Their Fig. 7, however, shows a positive shift at low temperature and a negative shift above ~ 60K. The values plotted in this graph are reproduced from their Eq. 19 and the parameters listed in their Table 6, but it appears that a negative sign in their equation was omitted (a factor of Loschmidt's number is also needed in their Eqs. 18 and 19 to obtain the reported values in their Fig 7 and Table 7). When these issues are taken into consideration, the present shift values and the Drouin et al. results, confirm this picture of a change in the pressure shift direction at temperatures near 60 K.

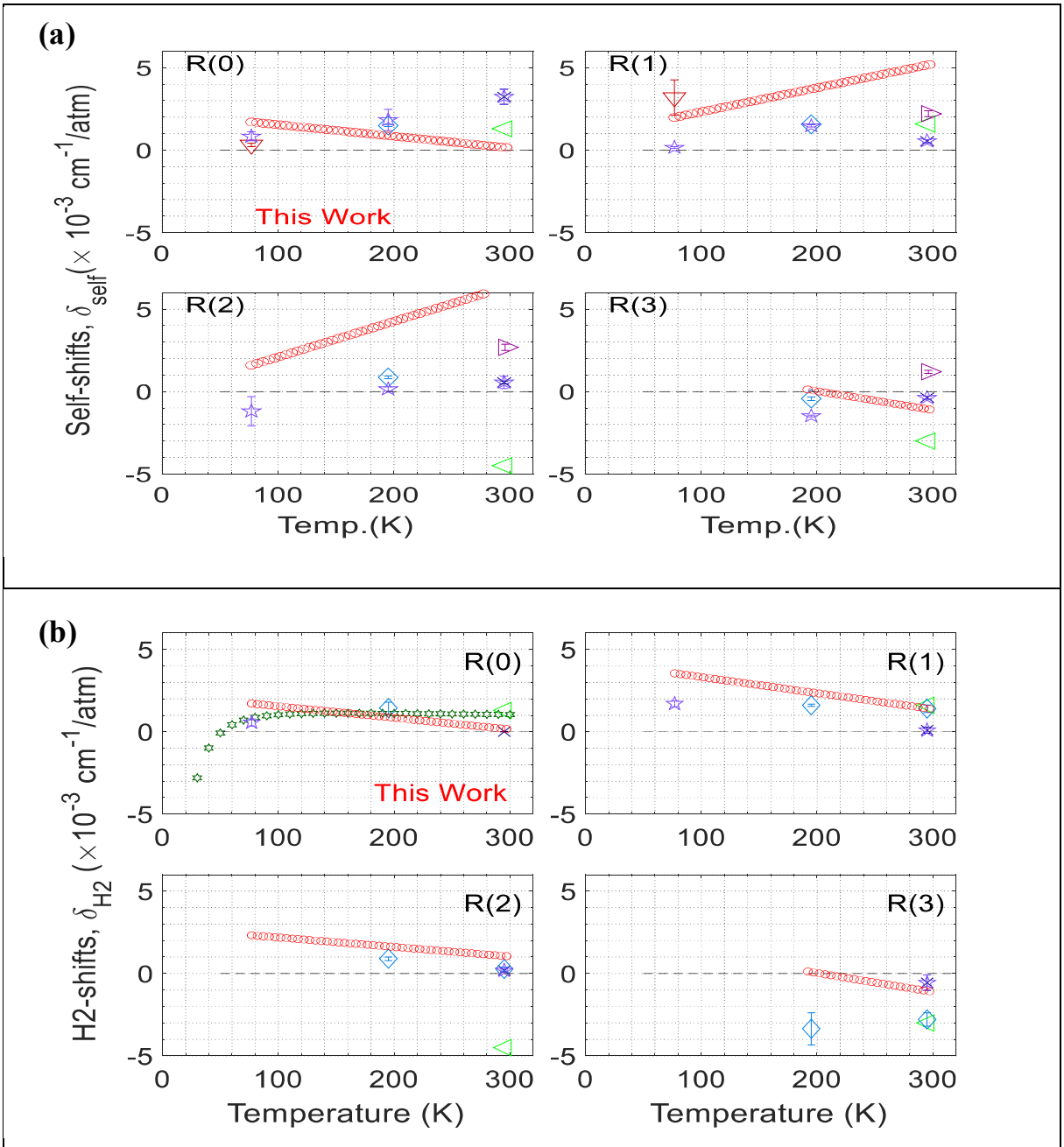

Fig. 7 Comparison of (upper) Self- and (lower) H_2-frequency shifts with pressure (cm^{-1}/atm). The symbols are for HITRAN 2020 (□), Feu13(◁), McK84 (▽), McK86(▷), Dra87(x), Uli89(☆), Lu93(◊), SM92 (hexagram), and this work (○). Note that HITRAN 2020 values are not available.

4.4.3 Collisional narrowing

The collisional (Dicke) narrowing effect has been studied in various molecules [Dic53; Gal61; Rau67; DeC84; Var84; Bra03; Weh06; *refs. therein*], and it was observed in pure HD spectra for the R(3) and R(6) transitions [Ess84]. These previous room temperature experiments at low pressures showed minimum linewidths at pressures where the magnitudes of the Doppler broadening and pressure broadening are comparable. The collisional narrowing effect is small and more pronounced for R(6) than R(3) as the Doppler broadening increases with the transition frequency. In the present work, narrowing parameters β (defined by Eq. 3b) have been retrieved for the R(1) and R(2) transitions to be 0.017(10) and 0.033(15) cm^{-1}/atm, respectively, without considering their temperature dependence. The narrowing parameter for the R(0) line was not well constrained. For the R(3) transition, a small value was retrieved, comparable to the error in the fit.

It is interesting that the narrowing parameters are greater than the broadening parameters by a factor of 1.5 to 3. A similar situation was found for line narrowing by Nazemi et al. [Naz83] in the HD fundamental band and by Wcisło et al. [Wci16] in the H_2 fundamental bands. A comparison of the present line narrowing can be made to a value of the 'optical' diffusion constant proposed by Pine [Pin92], D_{opt} [cm^2/s] = $k_B T/[2\pi mc\times(P\times\beta)]$, where k_B is the Boltzmann constant, m is the mass of HD, c is speed of light, P is pressure in atm, and β is the narrowing parameter in cm^{-1}/atm at 296 K. Using a mass diffusion coefficient value of 1.40 cm^2/sec, for a HD+H_2 mixture [Wei62], the line narrowing parameter is computed to be ~0.031. Hence, the new measurements are close to, or smaller than, the derived value by a factor of ~1.0 - 1.8. Note, however, that the mass diffusion constant is an aggregate property of the system, while narrowing parameters are transition specific.

5. Measurement errors for line strengths and line shape parameters

As discussed in Sec. 4.1, the retrieval errors presented in Table 4 are the errors that result from the fitting process alone. Further analysis has been conducted to assess the systematic uncertainty of each parameter due to the uncertainties of the experimental conditions and spectral measurements.

The uncertainty of the line intensity measurements is a combination of two categories of uncertainties given by Eqs. 8a and 8b, i.e. the uncertainty of the sample temperature, and the combined uncertainties of the transmission, mixing ratio, pressure, and pathlength. Since the line intensity $\boldsymbol{S}$ expressed by Eq. A1 is an implicit function of the temperature $\boldsymbol{T}$, the total partition function $\boldsymbol{Q}$, and the transition-specific lower state energy $\boldsymbol{E''}$, *etc.*, the impact on the line intensity retrieval is estimated from temperature measurement errors of ±1 K as presented in Table 2. The fractional uncertainties in the intensity due to temperature offsets are given by Eq. 8a. and shown in Fig 8a as a solid line within the measured temperature range and as a dashed line for extrapolated temperatures. The uncertainties range from 1 – 3.5 % depending on the HD transition and the measurement temperature.

$$\left(\frac{\delta S}{S}\right)_a = \frac{S(T+1)}{S(T)} - 1 \text{ or } \frac{S(T-1)}{S(T)} - 1 \qquad \text{(Eq. 8a)}$$

$$\left(\frac{\delta S}{S}\right)_b \cong \sqrt{\left(\frac{\delta\tau}{\tau}\frac{1}{ln\,\tau}\right)^2 + \left(\frac{\delta\xi}{\xi}\right)^2 + \left(\frac{\delta p}{p}\right)^2 + \left(\frac{\delta l}{l}\right)^2}. \qquad \text{(Eq. 8b)}$$

Table 6. The uncertainties of the line intensity S from Eqns 9a and 9b

Transition	$\left(\frac{\delta S}{S}\right)_a$ in %	SNR	τ range	$\left(\frac{\delta S}{S}\right)_b$ in %	No of Spec	Meas. unc.
R(0)	1.2	73	0.1 - 0.7	~ 4	15	1.5
R(1)	0.5	188	0.1 - 0.7	~1.5	17	0.5
R(2)	3.1	159	0.2 - 0.7	~ 2	17	1.0
R(3)	1.5	184	0.4 - 0.7	~ 1.5	7	1.0

The uncertainty resulting from the rest of the experimental conditions is estimated using the approach of Sung et al. [Sun09] and Varanasi and Chudamani [V&C89]. The observed transmission τ at the line center can be written as $\boldsymbol{\tau = e^{-c_0 \cdot S \cdot \xi \cdot p \cdot l}}$, where S is the line strength, ξ and p are the mixing ratio and pressure of the sample, l is the path length, and c_0 is a normalization constant of the line shape profile. After taking the logarithm on both sides and rearranging, the measurement uncertainty for the line strength can be related to the spectral signal-to-noise (SNR) and the experimental conditions expressed in Eq. 8b for a single spectrum case. The value of $\delta\tau$ in Eq. 8b is estimated from the reciprocal of the SNR of the HD spectra listed in Table 6. The uncertainties of the HD mixing ratios, the pressure readings, and the pathlength determination are less than 0.2% each. By substituting these values into Eq. 8b, the intensity uncertainty is 4% or less for HD transitions with transmissions in the range 10 to 70%, as in the presently analyzed spectra. Finally, these estimates are for the case of a single spectrum. Since line parameters are obtained by fitting multiple spectra simultaneously, the statistical uncertainties are further reduced by the square root of the number of spectra acquired for each transition. The resultant line intensity uncertainties are presented in Table 6, and they are assumed to be accurate for the measured temperatures in the range 98–298 K.

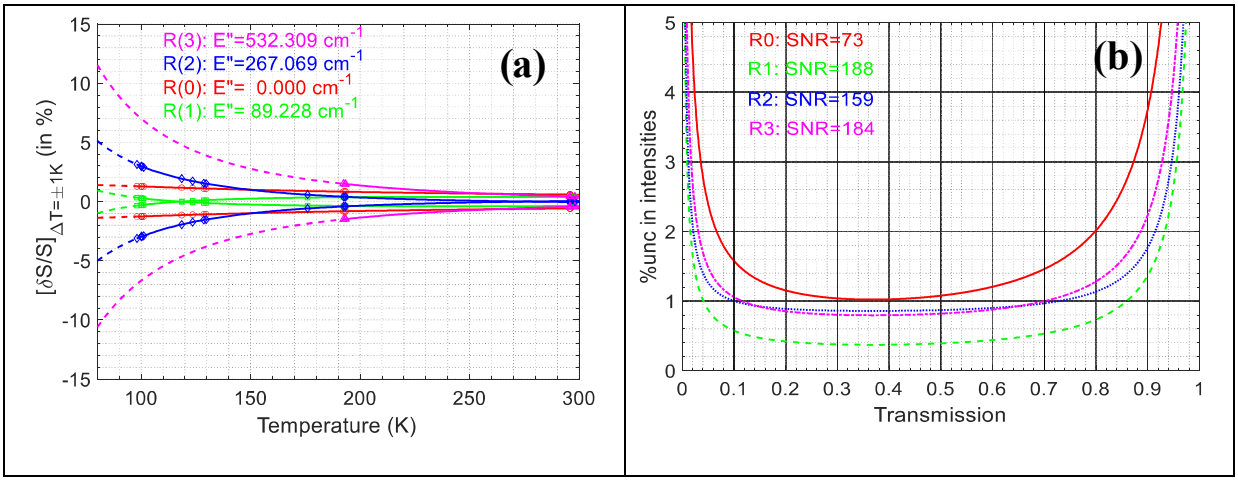

Fig. 8 (a) Line intensity uncertainties propagated from temperature errors of ±1 K at temperatures within (solid line) and outside (dashed line) the measured range. (b) The net combined intensity uncertainties from Eq. 8a&b weighted by square root of the number of spectra, which correspond to 1.5, 0.5, 1.0, 1.0% for the R(0) - R(3) transitions, respectively.

Line width and frequency shift errors are assessed as described in Benner et al. [Ben16]. Since these parameters define the molecular line shape profile, and are retrieved simultaneously, they are intrinsically coupled. In addition, their temperature dependence parameters are also retrieved simultaneously based on the empirical model (See Eqs. 4 and 5). The correlation coefficients reported by the multispectrum fitting package, Labfit [Ben95, Let07, Dro17], accounts for these couplings as part of the fitting solutions. Benner et al. [Ben16] gives the measurement uncertainties for the line widths in Eq. 9a, and the shift uncertainties in Eq. 9b.

$$\epsilon_{\gamma^0}^2(T) = \gamma^0(T_0)^2 \times \left\{ \frac{\epsilon_{\gamma^0(T_0)}^2}{\gamma^0(T_0)^2} + \ln\left(\frac{T_0}{T}\right)^2 \epsilon_n^2 + 2\rho_{\gamma^0(T_0),n} \times \frac{\ln\left(\frac{T_0}{T}\right)\epsilon_{\gamma^0(T_0)}\epsilon_n}{\gamma^0(T_0)} \right\} \quad \text{(Eq. 9a)}$$

$$\epsilon_{\delta^0}^2(T) = \delta^0(T_0)^2 + (T - T_0)^2\epsilon_{\delta'}^2 + 2\rho_{\delta^0(T_0),\delta'}(T - T_0)\epsilon_{\delta^0(T_0)}\epsilon_{\delta'} \quad \text{(Eq. 9b),}$$

where the ϵ's are the retrieval errors presented in Table 4, and ρ's are the correlation coefficients determined from the line parameter retrievals listed in Table 7. It should be noted that these correlation coefficients reflect constraints on parameters assuming the line shape model adopted in this work.

Table 7. The correlation coefficients ρ between the line width (γ^0) and pressure shifts (δ^0) and their corresponding temperature dependence parameters, n and δ'.

Transitions	$\rho_{\gamma^0(T_0),n}$ for H_2-widths	$\rho_{\gamma^0(T_0),n}$ for Self-widths	$\rho_{\delta^0(T_0),\delta'}$ For H_2-shifts	$\rho_{\delta^0(T_0),\delta'}$ For Self-shifts
R(0)	-0.7019	←	0.7693	←
R(1)	-0.6916	←	0.9339	0.1363
R(2)	-0.5191	←	0.7150	0.2391
R(3)	-0.5380	←	0.0666	←

The measurement uncertainties for the line widths are presented in Fig. 8a, which shows values varying between 1 – 8% for self-widths, and 1 – 4 % for H_2-widths, depending on transitions and temperatures. Fig. 8b shows that shift uncertainties increase as temperatures decrease, amounting to ~50% at the lowest temperatures. Figure 10 shows the line shift as a function of temperature overlaid with the measurement uncertainties.

Recall that line shape parameters and retrieval errors presented in Table 4 are the values at the reference temperature at 296 K. Their uncertainties are expected to vary with the temperature, as given in Eqs. 9a and 9b, and it is these uncertainties which are the realistic values for the line shape parameters.

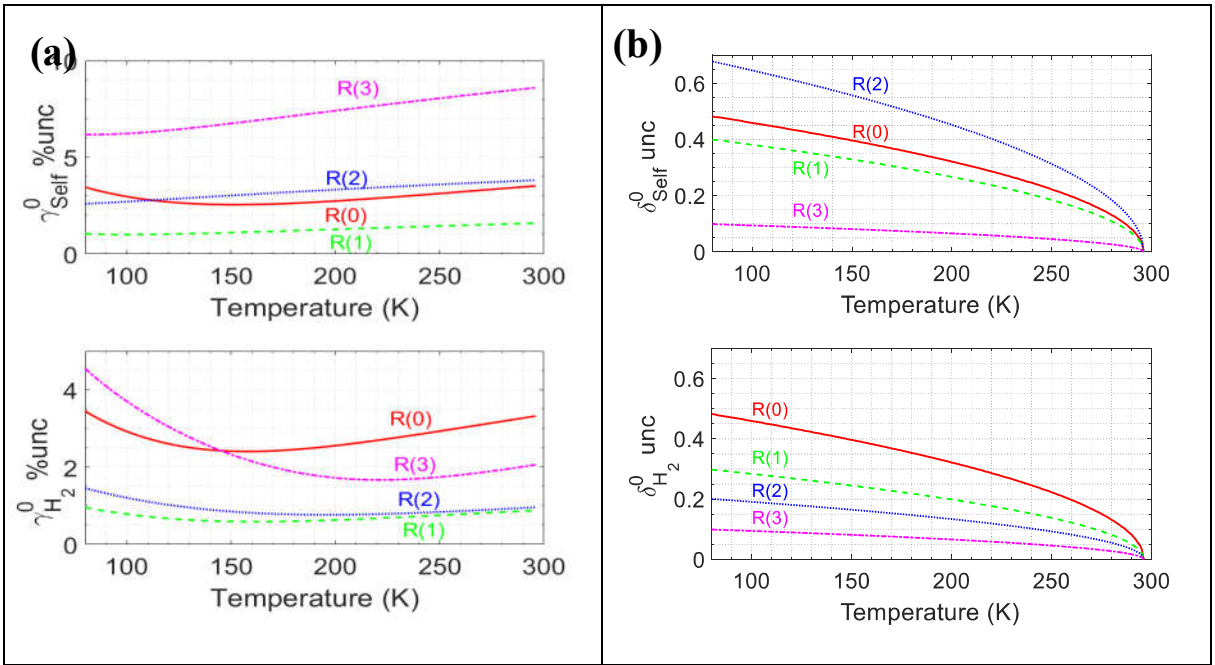

Fig. 9. (a) Measurement uncertainties (in %) for the Self- and H_2-widths (top and bottom, respectively) as a function of temperature, (b) Measurement uncertainties for the for the Self- and H_2- frequency shifts (top and bottom) in 10^{-3} cm^{-1}/atm as a function of temperature.

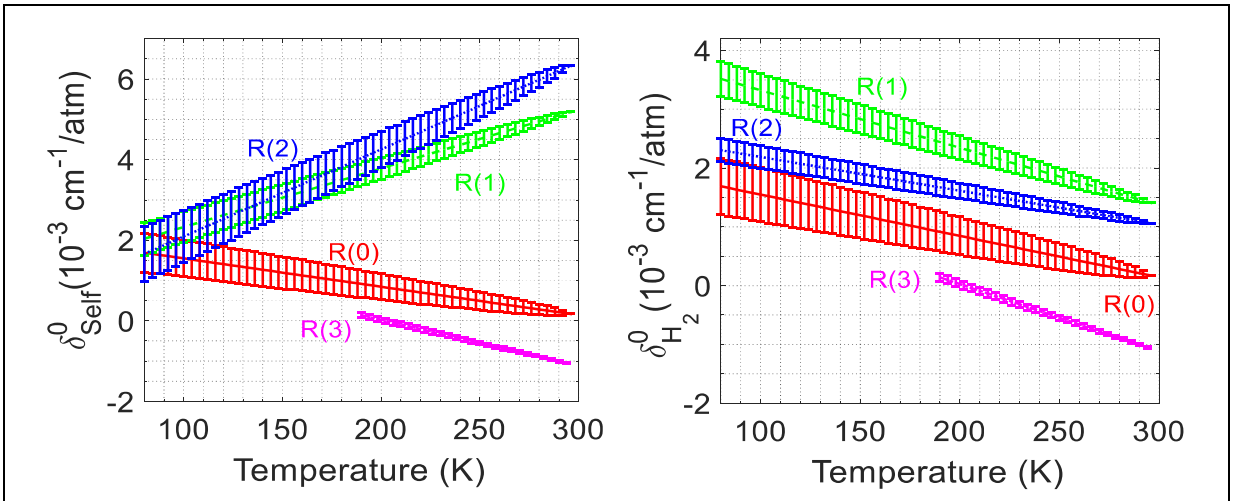

Fig. 10. Self-shifts and H_2-shifts (left and right) as a function of temperature with overlaid uncertainty estimates (Also see Fig. 7).

6. Conclusion

New measurements of the pure rotational spectra of HD and HD-H_2 mixtures have been obtained at temperatures between 98 and 296 K, at pressures below 1 atm. Multispectral fitting analysis of the data using a non-Voigt line shape yields spectroscopic parameters for the R(0) - R(3) transitions of HD. These parameters are in general agreement with previous work, however notably, the pressure-broadened linewidths reported here, and previously, are a factor of 5 less than those listed in the HITRAN and GEISA databases. Note that the databases also have the value 0.05 cm^{-1}/atm for the H_2 rotational linewidths, and these also need correction [DeC84, Reu94]. The low temperature and low pressure experimental conditions used here are closer to the conditions found in the atmospheres of the giant gaseous planets than have been used previously. As such, the present results are particularly relevant to the interpretation of planetary spectra and should be valuable to planetary science.

Acknowledgments:

Part of the research described in this manuscript was performed at the Jet Propulsion Laboratory, California Institute of Technology, and was supported by PDART program under the National Aeronautics and Space Administration. Data acquisition on the AILES beamline at the Synchrotron Soleil was granted under Projects (20180459 and 20190213). C. Nixon acknowledges support from the Fundamental Laboratory Research (FLaRe) program within the NASA Internal Scientist Funding Model (ISFM).

We dedicate this paper to the memory of Irving Ozier (1938-2022), with appreciation for his contributions to molecular spectroscopy, and to members of this research collaboration.

Appendix: The relationship between the line intensity and the dipole moment

The multispectrum fit yields the line intensity, S, (cm^{-1}/(molecule·cm^{-2})) at 296 K in the HITRAN formulation (see the HITRAN96 appendix [Rot98], Gamache and Rothman [Gam92], and Simečková et al. [Sim06]). S is listed in the HITRAN database at 296 K and from this quantity one can calculate a synthetic spectrum. The physical property of the molecular dipole moment can be derived from the line intensity $\boldsymbol{S_{JJ'}}$(T) where it is defined by:

$$\boldsymbol{S_{JJ'}(T)} = \left(\frac{8\pi^3}{3hc}\right)\boldsymbol{\nu_{JJ'}}\frac{\boldsymbol{I_a g_{J,total}}\exp\left(-\frac{c_2 E_J}{T}\right)}{\boldsymbol{Q(T)}}\left[\mathbf{1}-\exp\left(-\frac{c_2\nu_{JJ'}}{T}\right)\right]\times\mathbb{R}_{JJ'} \qquad \text{(A.1)}$$

where $c_2 = hc/k = 1.4388$ cm·K, I_a is the isotopomeric abundance, $\boldsymbol{E_J}$ is the lower state energy, $\boldsymbol{\nu_{JJ'}}$ is the transition frequency, $\boldsymbol{T}$ is the temperature, h is Planck's constant, k is Boltzmann's constant, and c is the speed of light. The total internal partition function, $Q(T)$ is expressed by

$$Q = Q_{ele}Q_{vib}Q_{rot}Q_{tor}Q_{spin} \sim \sum_J g_J \exp\left(-\frac{c_2 E_J}{T}\right) \times g_{spin}. \quad \text{(A.2)}$$

In practice, we have used the total internal partition computed by the TIPS program [Gam17]. The statistical weighting factor, $\boldsymbol{g_{J,total}} = g_{angular} \times g_{spin} = (2J+1) \times g_{spin}$; $g_{spin} = (2\mathrm{H}+1) \times (2\mathrm{D}+1) = 6$ for HD. $\mathbb{R}_{JJ'}$ is the weighted square of the transition moment, which is independent of temperature, but dependent on J. Note the summation over the states ζ, ζ', as defined by

$$\mathbb{R}_{JJ'} \equiv \left(\frac{1}{g_J}\right) \sum_{\zeta,\zeta'} \left|R_{(J\zeta),(J'\zeta')}\right|^2. \quad \text{(A.3)}$$

Townes and Schawlow (Pgs. 22-23) [Tow75] show that the probability of absorption of randomly polarized radiation by randomly oriented molecules is a sum over the dipole moment matrix elements for a transition from states JM to $J'M'$

$$\left|\mu_{ij}\right|^2 = \sum_{M'} \left(|\mu_x(JMJ'M')|^2 + \left|\mu_y(JMJ'M')\right|^2 + |\mu_z(JMJ'M')|^2\right) \quad \text{(A.4)}$$

and the sum $\left|\mu_{ij}\right|^2$ for all J,M equals $\mu^2 \times \frac{(J+1)}{(2J+1)}$, for absorbing transitions in the R-branch, i.e. J+1←J, where μ^2 is the square of the molecular dipole moment and it is independent of J. Thus,

μ^2 is related to the HITRAN quantities above by

$$\mathbb{R}_{\boldsymbol{JJ'}} = \left(\frac{1}{g_J}\right) \sum_{\zeta,\zeta'} \left|R_{(J\zeta),(J'\zeta')}\right|^2 = \mu^2(J+1)/(2J+1). \quad \text{(A.5)}$$

Finally the relation between the line intensity and the dipole moment squared as shown in Eq 7 is:

$$S_{JJ'}(T) = \left(\frac{8\pi^3}{3hc}\right) \nu_{JJ'} \frac{I_a g_{spin}}{Q(T)} \exp\left(-\frac{c_2 E_J}{T}\right) \left[1 - \exp\left(-\frac{c_2 \nu_{JJ'}}{T}\right)\right] \times \mu^2(J+1) \quad \text{(Eq. 7)}$$

References

[Abb10] Abbas MM, Kandadi H, LeClair A, et al. D/H ratio of Titan from observations of the Cassini/Composite Infrared Spectrometer. ApJ, 2010; 708: 342 – 353.

[Alt15] Altwegg K, et al. 67P/Churyumov-Gerasimenko, a Jupiter family comet with a high D/H ratio. Science, 2015; 347, 6220, 1261952-1.

[Ben95] Benner DC, Rinsland CP , Devi MV, Smith MAH, Atkins D. A multispectrum nonlinear least squares fitting technique. J Quant Spectrosc Radiat Transfer 1995;53:705–21.

[Ben16] Benner DC, Devi VM, Sung K, et al. Line parameters including temperature dependences of air- and self-broadened line shapes of $^{12}C^{16}O_2$: 2.06-μm region. J Mol Spectrosc 2016; 326: 21 – 47.

[Bez86] Bézard B, Gautier D, Marten A. Detectability of HD and non-equilibrium species in the upper atmospheres of the giant planets from their submillimeter spectrum. A&A 1986; 161: 387.

[Bra03] Brault JW, Brown LR, Chackerian Jr C, Freedman R, Predoi-Cross A, Pine AS. Self-broadened $^{12}C^{16}O$ line shapes in the v = 2, 0 band. J Mol Spectrosc 2003; 222:220-239.

[dBe86] de Bergh C, Lutz CJ, et al. Monodeuterated methane in the outer solar system. II - Its detection on Uranus at 1.6 microns. ApJ 1986; 311: 501.

[dBe90] de Bergh C, Lutz BL, Owen T, et al. Monodeuterated methane in the outer solar system. IV - Its detection and abundance on Neptune, ApJ 1990; 355: 661.

[Cza18] Czachorowski P, Puchalski M, Komasa J, Pachucki K. Nonadiabatic relativistic correction in H_2, D_2, and HD. Physical Review A 2018; 98, 052506.

[DeC84] De Cosmo V., Gush HP, Halpern M, The $S_0(1)$ quadrupole line of H_2, Can J Phys 62, 1713 (1984)

[Dev10] Devi VM, Benner DC, Rinsland CP, et al. Multispectrum measurements of spectral line parameters including temperature dependences of N_2- and self-broadened half-width coefficients in the region of the ν_9 band of $^{12}C_2H_6$. J Quant Spectrosc Radiat Transfer 2010 ; 111: 2481 - 2504.

[Dev16a] Devi VM, Benner DC, Sung K, et al. Line parameters including temperature dependences of self- and air-broadening line shapes of $^{12}C^{16}O_2$: 1.6 μm region. J. Quant. Spectrosc. Radiat. Transfer 2016a; 177: 117 - 144.

[Dev16b] Devi VM, Benner DC, Sung K, et al. Spectral line parameters including line shapes in the $2\nu_3$ Q branch of $^{12}CH_4$. J. Quant. Spectrosc. Radiat. Transfer 177, 152 - 169 (2016b).

[Dic53] Dicke RH. The effect of collisions upon the Doppler width of spectral lines. Phy. Rev. 1953; 89: 472 – 473.

[Dra87a] Drakopoulos PG, Tabisz GC. Far-infrared rotational spectrum of HD: Line shape, dipole moment, and collisional interference. Phys. Rev. A. 1987a; 36: 5556 – 5565.

[Dra87b] Drakopoulos PG, Tabisz GC. Collisional interference in the foreign-gas-perturbed far-infrared rotational spectrum of HD. Phys. Rev. A. 1987b; 36: 5566 – 5574.

[Dro11] Drouin BJ, Yu S, Pearson JC, Gupta H. Terahertz Spectroscopy for Space Applications, 2.5-2.7: THz Spectra of HD, H_2O and NH_3. J. Mol. Struct. Special Issue on THz Spectroscopy, 2011; 1006: 2-12.

[Dro17] Drouin BJ, Benner DC, Brown LR, et al. Multispectrum analysis of the oxygen A-band. J. Quant. Spectrosc. Radiat. Transfer 2017; 186: 118 - 138.

[Enc96] Encrenaz Th, de Graauw Th, Schaeidt S. First results of ISO-SWS observations of Jupiter. Astron Astrophys 1996; 315: L397–L400.

[Ess84] Essenwanger P, Gush HP. Rotational spectrum of HD at low pressures, Can J Phys 1984; 62: 1680.

[Evn88] Evenson KM, Jennings DA, Brown JM, Zink LR, et al. Frequency measurement of the J = 1 – 0 rotational transition of HD. Astrophys J 1988; 330: L135–L136.

[Fan63] Fano U. Pressure Broadening as a Prototype of Relaxation. Phys. Rev. 1963; 131: 259.

[Feu99] Feuchtgruber H, Lellouch E, Bezard B, et al. Detection of HD in the atmospheres of Uranus and Neptune: a new determination of the D/H ratio, A&A 1999; 341: L17–L21.

[Feu13] Feuchtgruber H, Lellouch E, Orton G, et al. The D/H ratio in the atmospheres of Uranus and Neptune from Herschel-PACS observations, A&A 2013; 551: A126.

[For77] Ford AL, Browne JC. Ab initio calculation of line strengths in electric-dipole vibration-rotation spectrum of HD molecule. Phys. Rev. A 1977; 16: 1992.

[Gal61] Galatry L. Simultaneous Effect of Doppler and Foreign Gas Broadening on Spectral Lines. Phys Rev 1961; 122: 1218.

[Gam17] Gamache RR, Roller C, Lopes E, Gordon IE, Rothman LS, et al. Total internal partition sums for 166 isotopologues of 51 molecules important in planetary atmospheres: Application to HITRAN 2016 and beyond. J. Quant. Spectrosc. Radiat. Transfer 2017; 203: 70 – 87.

[Gam92] Gamache RR, Rothman LS.Extension of the HITRAN database to non-LTE applications. J. Quant. Spectrosc. Transfer 1992; 48: 519 - 525.

[Gor22] Gordon IE, Rothman LS, Hargreaves RJ, Hashemi R, Karlovets EV, et al. The HITRAN2020 Molecular Spectroscopic Database. JQSRT 2022; 277: 107949. doi:10.1016/j.jqsrt.2021.107949.

[Gri96] Griffin M, Naylor D, Davis G, et al. First detection of the 56-µm rotational line of HD in Saturn's atmosphere, A&A 1996; 315: L389-L392.

[Hum82] Humlicek J. Optimized computation of the Voigt and Complex probability functions. JQSRT 1982; 27: 437-44.

[Jaq10] Jacquemart D, Gomez L, Lacome N, Mandin J-Y, Pirali O, Roy P. J. Quant. Spectrosc. Radiat. Transfer 2010; 111: 1223–1233.

[Jac16] Jacquinet N , et al. The 2015 edition of the GEISA spectroscopic database. J Molec Spectrosc 2016; 327:31–72.

[Joz20] Józwiak H, Cybulski H , Wcisło P. Positions and intensities of hyperfine components of all rovibrational dipole lines in the HD molecule. JQSRT 2020; 253, 107171. https://doi.org/10.1016/j.jqsrt.2020.107171

[JPL Catalog] https://spec.jpl.nasa.gov/

[Kom19] Komasa J, Puchalski M, Czachorowski P, Łach G, Pachucki K. Rovibrational energy levels of the hydrogen molecule through nonadiabatic perturbation theory. Phys Rev A 2019;100:032519. doi: 10.1103/PhysRevA.100.032519.

[Léc96] Lécluse C, Robert F, Gautier D, Guiraud M. Deuterium enrichment in giant planets, Planet. Space Sci. 1996; 44 : 1579-1592.

[Lel01] Lellouch E, Bezard B, Fouchet T, et al. The deuterium abundance in Jupiter and Saturn from ISO-SWS observations, A&A 2001; 670: 610.

[Let07] Letchworth KL, Benner DC. Rapid and accurate calculation of the Voigt function. J. Quant. Spectrosc. Radiat. Transfer 2007; 107: 173-192.

[Lu 93] Lu Z, Tabisz G, Ulivi L. Temperature dependence of the pure rotational band of HD: Interference, widths, and shifts, Phys Rev A, 1993; 47, 1159 – 1173.

[Ma85] Ma Q, Tipping R, Poll J. Mixing of rotational levels and intracollisional interference in the pure rotational R0(J) transitions of gaseous HD. Phys Rev A, 1985; 38: 6185 – 6189.

[Man19] Laurent Manceron of Synchrotron Soleil, France, *Private Comm.*

[McK84] McKellar ARW, Johns JWC, Majewski W, et al. Interference effects in the spectrum of HD: III. The pure rotational band at 77 K for HD and HD-Ne mixtures. Can. J. Phys. 1984; 62: 1673 – 1679.

[McK86] McKellar ARW. Interference effects in the spectrum of HD: IV: the pure rotational band at room temperature, Can. J. Phys. 1986; 62: 227 – 231.

[Mou04] Mousis O. An estimate of the D/H ratio in Jupiter and Saturn's regular icy satellites – Implications for the Titan Huygens mission, A&A 2004; 414: 1165–1168.

[Naz83] Nazemi S., Javan A, Pine A.S. Collisional effects on the rovibrational transitions of the HD fundamental band. J. Chem. Phys. 1983; 78: 4797 – 4805.

[Nel82] Nelson J, Tabisz G. New Spectroscopic Determination of the Dipole Moment of HD in the Ground Vibrational State. Phys Rev A, 1982; 48: 1393 – 1396.

[Nel83] Nelson J, Tabisz G. Intracollisional interference in the pure rotational spectrum of HD: Determination of the permanent electric dipole moment, Phys Rev A 1983; 28: 2157 – 2161.

[Pie17] Pierel JDR, Nixon CA, Lellouch E, Fletcher LN, Bjoraker GL, Achterberg RK, Bézard B, Hesman BE, Irwin PGI, Flasar FM. D/H Ratios on Saturn and Jupiter from Cassini CIRS. Astronomical J 2017; 155: 178 – 190.

[Owe92] Owen T. Deuterium in the Solar System, in "Astrochemistry of Cosmic Phenomena", Ed. P. Singh (Dordrecht: Kluwer), p.97 (1992).

[Pac08] Pachucki K, Komasa J. Electric dipole rovibrational transitions in the HD molecule. Physical Review A 2008; 78: 052503 - 7.

[Pac10] Pachucki K, Komasa J. Rovibrational levels of HD, Phys Chem Chem Phys. 2010; 12, 9188–96.

[Pic91] Pickett HM. The Fitting and Prediction of Vibration-Rotation Spectra with Spin Interactions. J. Mol. Spectrosc. 1991; 148, 371 – 377.

[Pin92] Pine A.S. Self-, N_2, O_2, H_2, Ar, and He broadening in the ν_3 band Q branch of CH_4. J. Chem. Phys. 1992; 97: 773 – 785.

[Pol76] Poll JD, Tipping RH, Prasad RDG, Reddy SP. Intracollisional Interference in the Spectrum of HD Mixed with Rare Gases. Phys. Rev. Lett. 1976; 36: 248.

[Pol85] Poll, J.D. The Infrared Spectrum of HD. In: Birnbaum, G. (eds) Phenomena Induced by Intermolecular Interactions. NATO ASI series. 1985; 127: Springer, Boston, MA. https://doi.org/10.1007/978-1-4613-2511-6_37

[Rau67] Rautian SG, Sobelman II. The effect of collisions on the doppler broadening of spectral lines. Soviet Phys. Uspheki 1967; 6: 701–716.

[Reu94] Reuter DC, Sirota JM, Line strength and self-broadening coefficient of the pure rotational S(1) quadrupole line in H_2,, ApJ, 428, L77-79 (1994)

[Rich83] Rich, NH, McKellar ARW, Interference effects in the spectrum of HD: I. The fundamental band of pure HD, Can. J. Phys. 1983; 61: 1648

[Rot96] Rothman LS, Rinsland CP, Goldman A, et al. The HITRAN molecular spectroscopic database and HAWKS (HITRAN Atmospheric Workstation) 1996 Edition. J. Quant. Spectrosc. Radiat. Transfer 1998: 60: 665 – 710.

[Rot13] Rothman LS, Gordon IE, Babikov Y, et al. The HITRAN 2012 Molecular Spectroscopic Database. J. Quant. Spectrosc. Radiat. Transfer, 2013; 130: 4 - 50.

[Sch87] Schwartz, C., Le Roy, R. Nonadiabatic eigenvalues and adiabatic matrix-elements for all isotopes of diatomic hydrogen, J Mol Spect 1987; 121: 420–39.

[SM92] Schaefer J, Monchick L. Line broadening of HD immersed in He and H_2 gas. Astron Astrophys 1992; 265: 859-868.

[Sim06] Simeckova M, Jacquemart D, Rothman LS, et al. Einstein A-coefficients and statistical weights for molecular absorption transitions in the HITRAN database. J. Quant. Spectrosc. Radiat. Transfer. 2006; 98: 130 – 155.

[Sun16] Sung K, Yu S, Pearson JC, et al. Far-infrared $^{14}NH_3$ line positions and intensities measured with a FT-IR and AILES beamline, Synchrotron SOLEIL, J Mol Spect, 2016a; 327: 1 – 20.

[Sun20] Sung K, Dev VM, Benner DC, Drouin BJ, Crawford TJ, Mantz AW, Smith MAH. H2-pressure broadening and frequency shifts of methane in the v2+v3 band measured in the temperature range between 80 and 370 K. JQSRT 2020; 255: 107264. https://doi.org/10.1016/j.jqsrt.2020.107264

[Tab85] Tabisz G, Nelson J. Rotational-level mixing and intracollisional interference in the pure rotational spectrum of HD gas, Phys Rev A, 1985; 31: 1160.

[Tch13] Kwabia Tchana F et al. A new, low temperature long-pass cell for mid-infrared to terahertz spectroscopy and synchrotron radiation use," Rev. Sci. Inst. 2013; 84, 093101.

[Tho85] Thorson WR, Choi JH, Knudson SK. Novel theory of the HD dipole moment. I. Theory. Phys. Rev. A 1985; 31: 22 and 31: 34.

[Tip78] Tipping H, Poll JD, McKellar ARW. The influence of intracollisional interference on the dipole spectrum of HD, Can. J. Phys. 56, 75 (1978).

[Tow75] Towns and Schawlow. Microwave Spectroscopy. Dover Publications, Inc. New York. 1975.

[Tre68] Trefler M, Gush HP. Electric dipole moment of HD, Phys Rev Lett 1968; 20: 703 – 705.

[Uli89] Ulivi L, Lu Z, Tabisz G. Temperature dependence of the collisional interference in the pure rotational far-infrared spectrum of HD, Phys. Rev. A 1989; 40 : 642.

[Uli91] Ulivi L, de Natale P. Inguscio, M., 1991. Pure rotational spectrum of hydrogen deuteride by far-infrared Fourier transform spectroscopy, ApJ. 1991; 378: L29 – L31.

[Var84] Varghese PL, Hanson RK. Collisional narrowing effects on spectral line shapes measured at high resolution. Appl. Opt. 1984; 23: 2376 – 2385.

[V&C89] Varanasi P, Chudamani S. Intensity and Line Width Measurements in the Fundamental Band of $^{13}CH_4$. J. Geophys. Res. 1989; 94: 11,175 – 11,178.

[Var90] Varanasi P, Chudamani S. The temperature dependence of lineshifts, linewidths and line intensities of methane at low temperatures. J. Quant. Spectrosc. Radiat. Transfer 1990; 43: 1 – 11.

[Wag67] Wagoner RV, Fowler WA, Hoyle F. On the synthesis of elements at very high temperatures. ApJ. 1967; 148: 3- 49.

[Wci16] P. Wcislo, I.E. Gordon, H. Tran, et al. The implementation of non-Voigt line profiles in the HITRAN database: H2 case study. J. Quant. Spectrosc. Radiat Transfer. 2016; 177: 75 – 91.

[Wei62] Weissman S., Mason E.A. Determination of Gaseous-Diffusion Coefficients from Viscosity Measurements. J. Chem. Phys. 1962; 37: 1289 – 1300.

[Wis92] Wishnow EH, Ozier I, Gush HP. Submillimeter spectrum of low temperature hydrogen: the pure translational band of H_2 and the R(0) line of HD. ApJ, 1992; 392: L43 – L46.

[Wol76] L. Wolniewicz. Nonadiabatic corrections to the rotational energies of the hydrogen molecule. Journal of Molecular Spectroscopy 1976; 63: 537-546.

[Wol83] Wolniewicz L. The $X^1\Sigma^+_g$ state vibration- rotational energies of the H_2 , HD, and D_2 molecules. The Journal of Chemical Physics 1983; 78:10, 6173-6181.

[Yu10] Yu S, Pearson JC, Drouin BJ, et al. Submillimeter-wave and far-infrared spectroscopy of high-J transitions of the ground and v_2=1 states of ammonia. J. Chem. Phys. 2020; 133: 174317.

Fig. 1

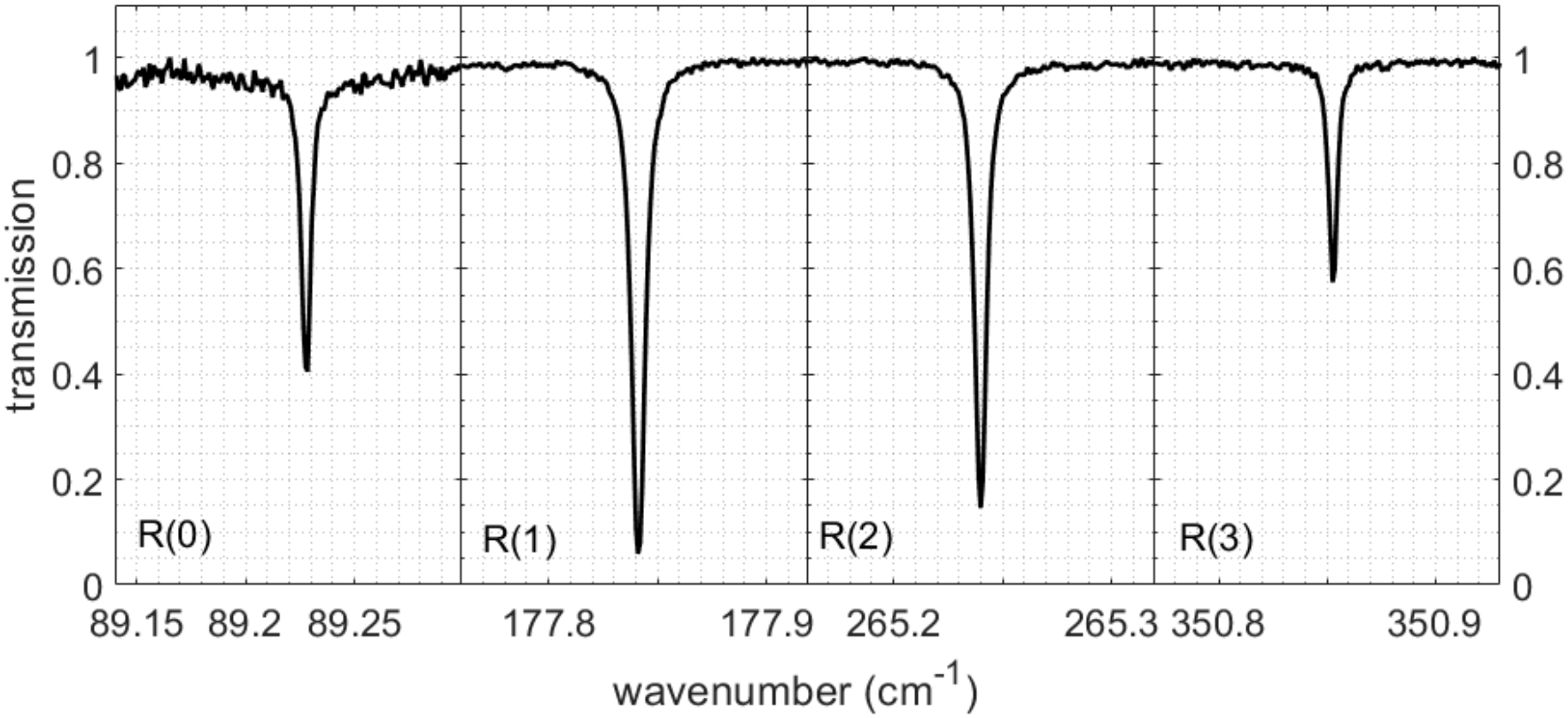

Fig.2

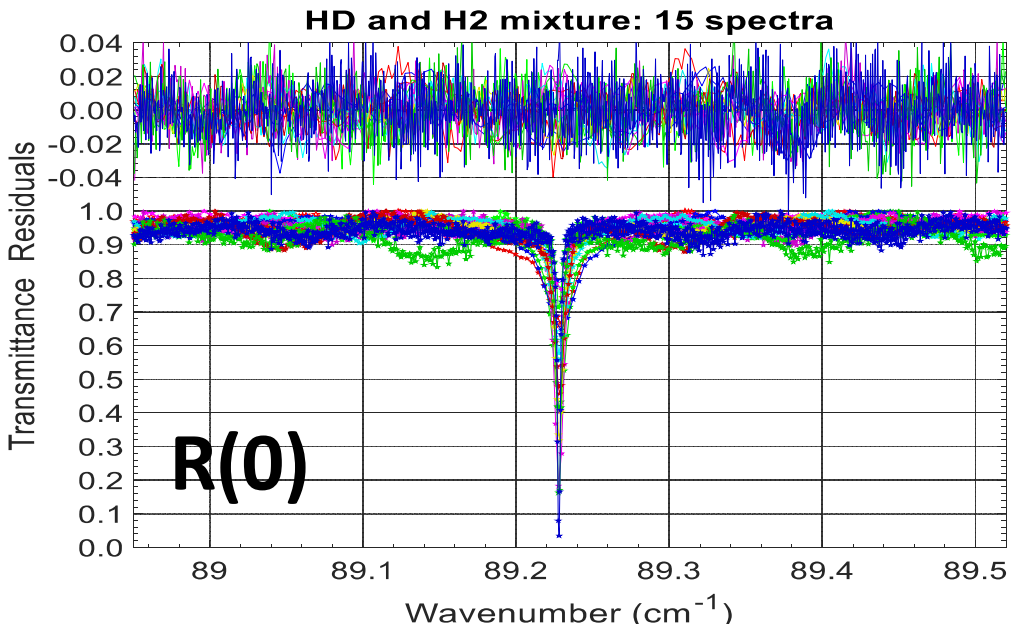
HD and H2 mixture: 15 spectra
Transmittance Residuals
Wavenumber (cm-1)
R(0)

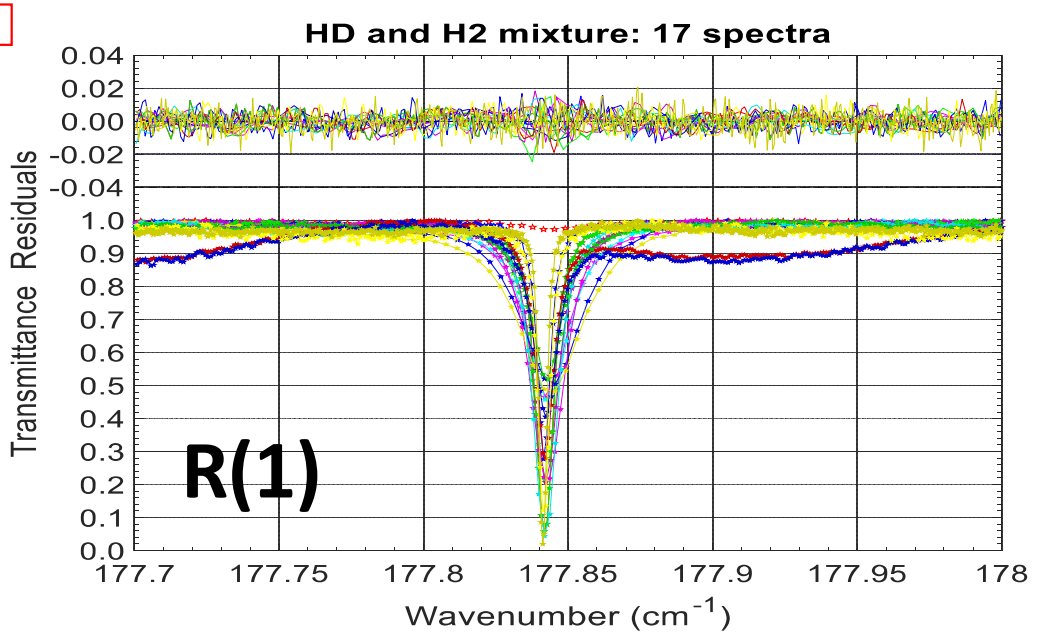
HD and H2 mixture: 17 spectra
Transmittance Residuals
Wavenumber (cm-1)
R(1)

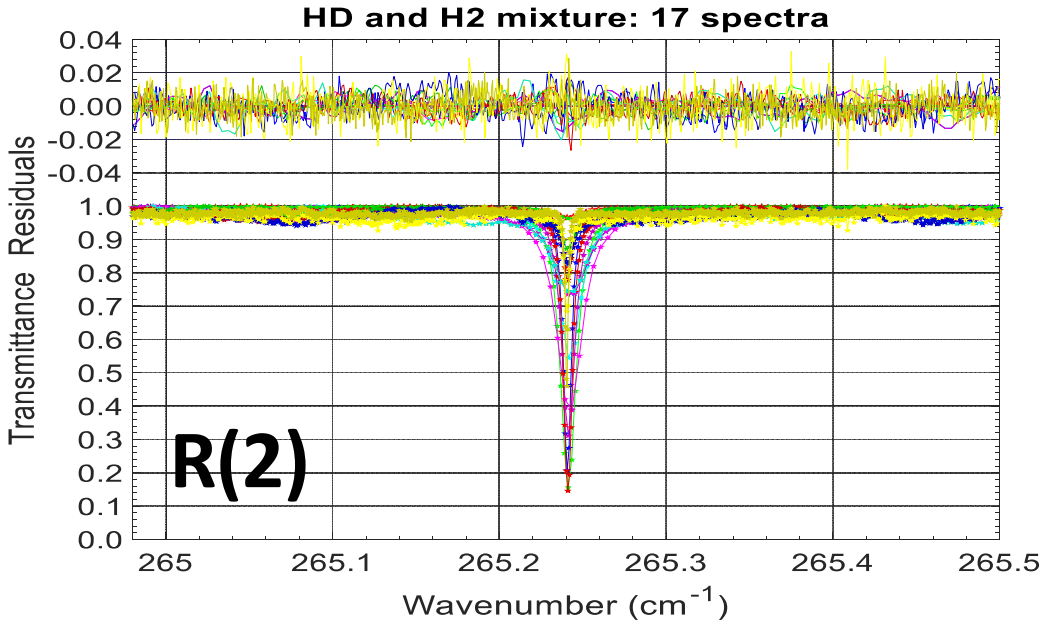
HD and H2 mixture: 17 spectra
Transmittance Residuals
Wavenumber (cm-1)
R(2)

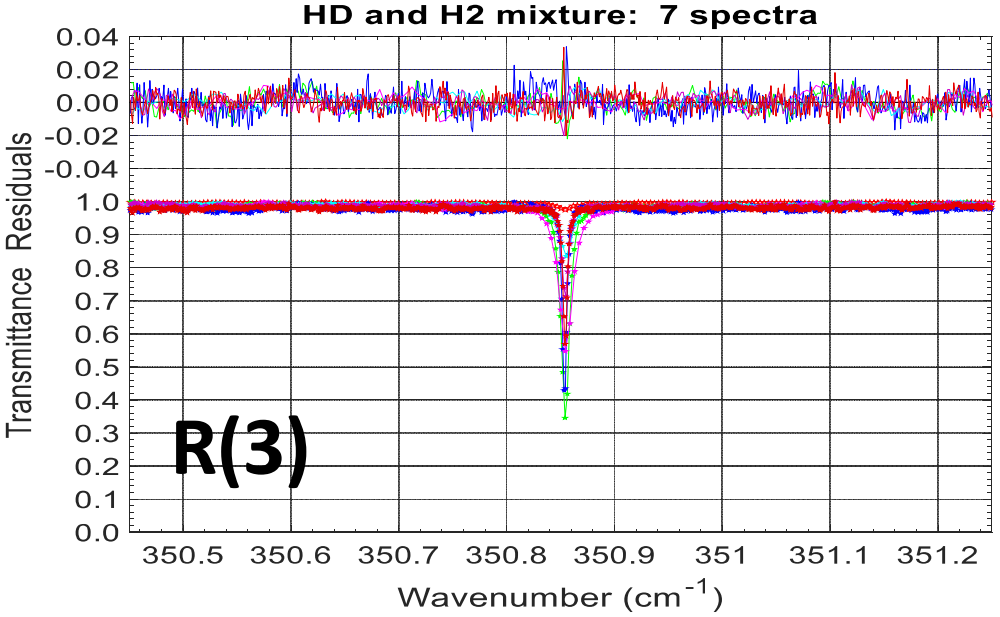
HD and H2 mixture: 7 spectra
Transmittance Residuals
Wavenumber (cm-1)
R(3)

Fig.3

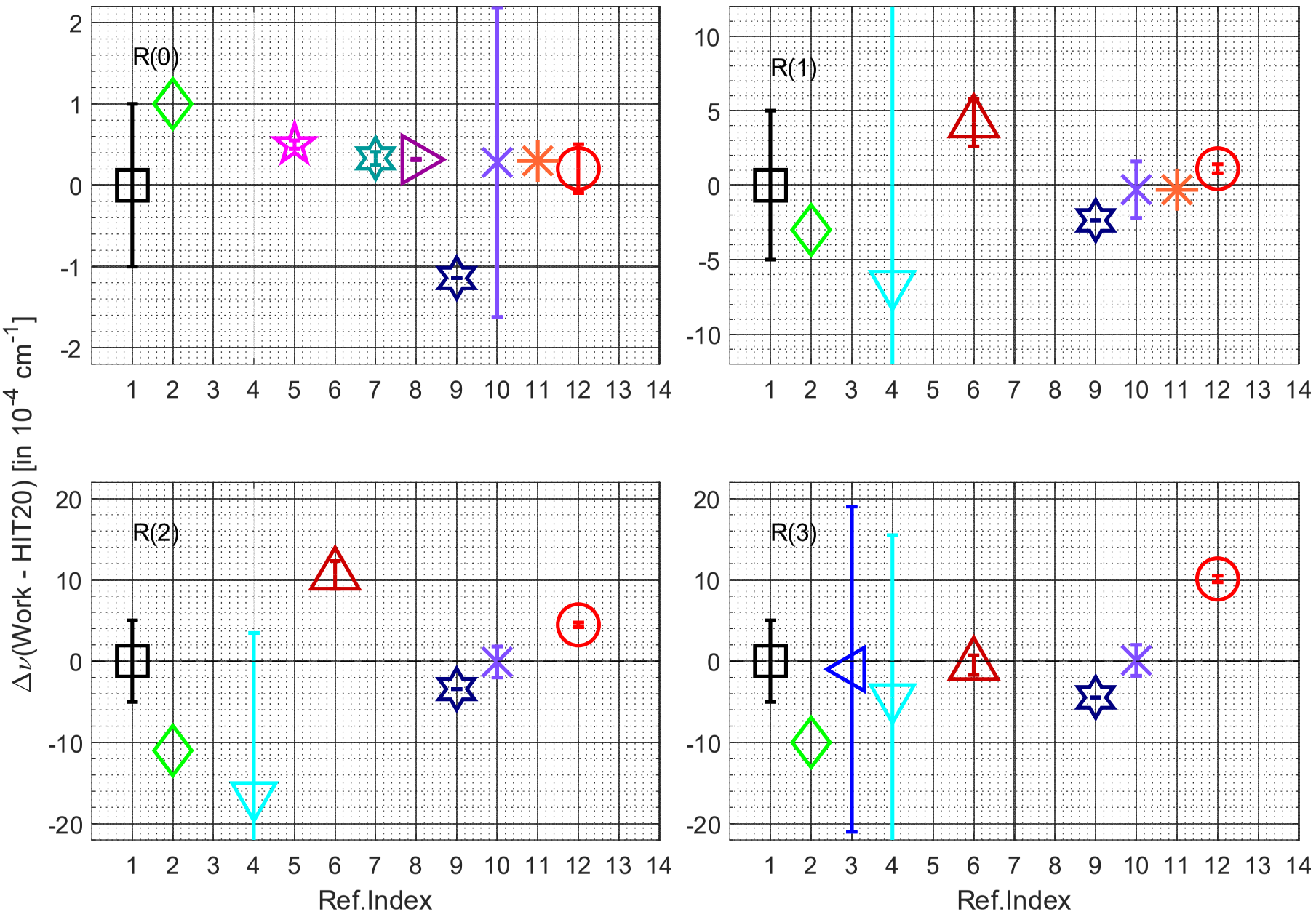

Fig. 4

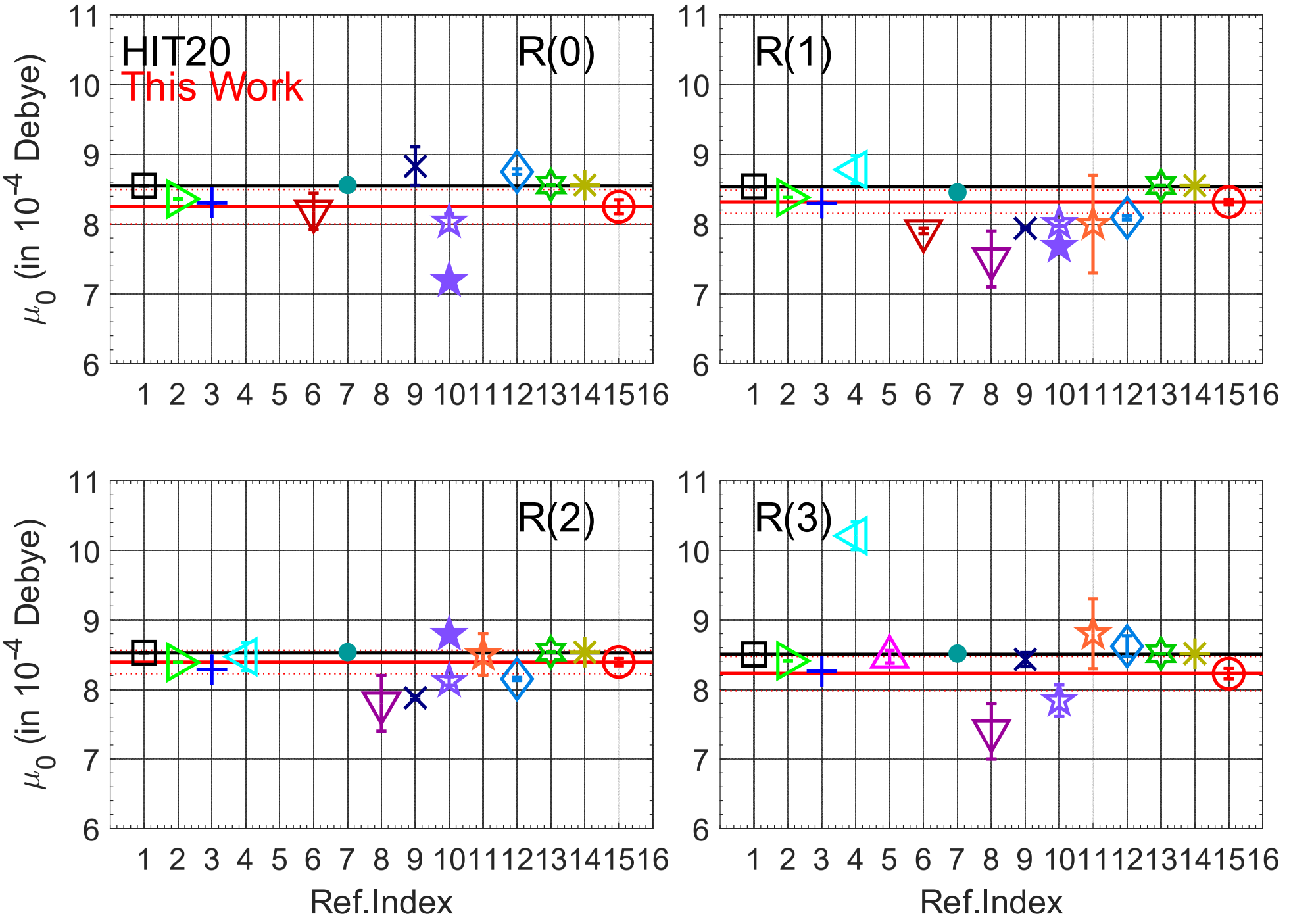
HIT20
This Work
R(0)
R(1)
R(2)
R(3)
μ_0 (in 10^{-4} Debye)
Ref.Index
11
10
9
8
7
6
1 2 3 4 5 6 7 8 9 10 11 12 13 14 15 16

Fig.5a

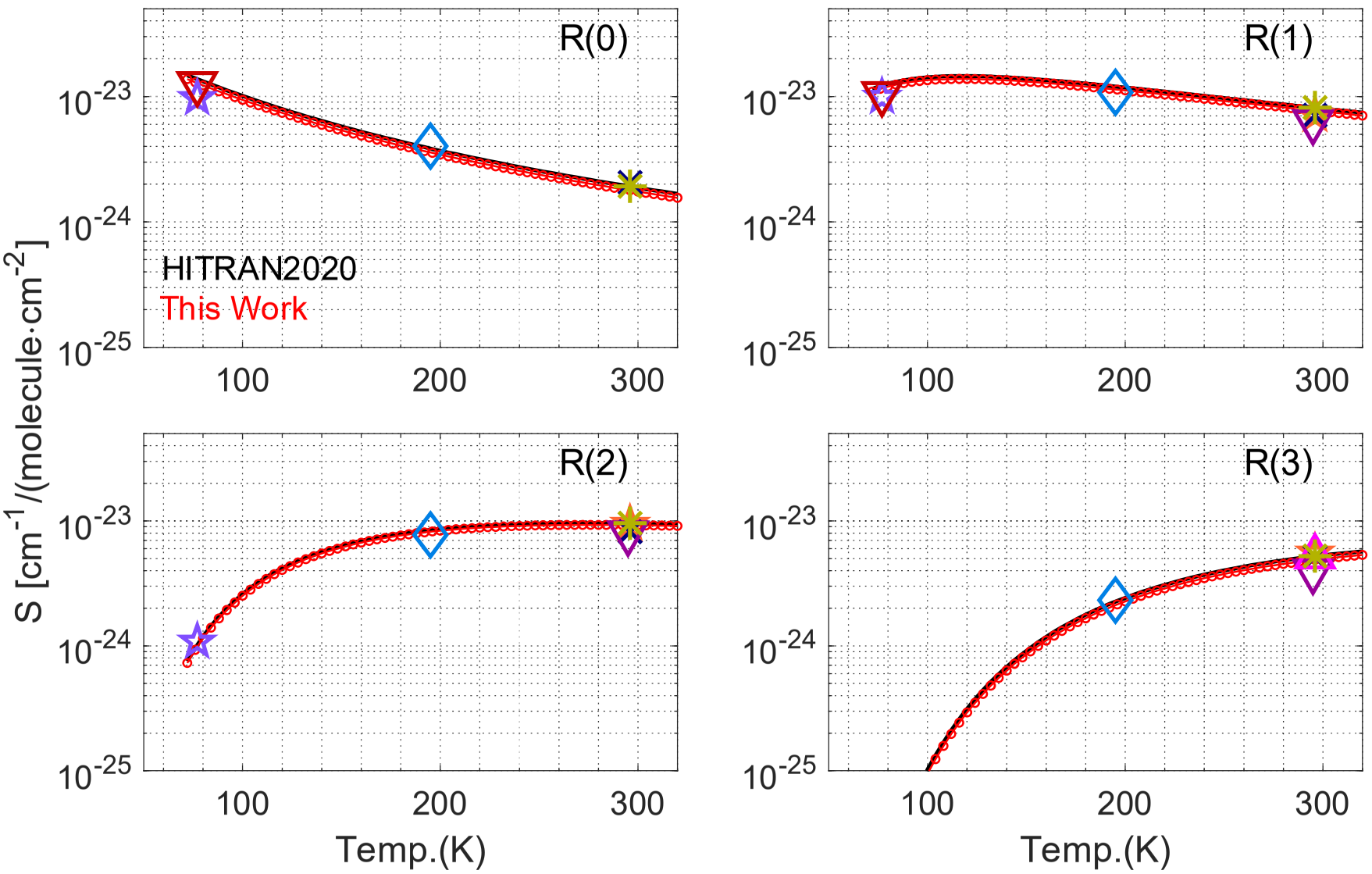
R(0)
R(1)
R(2)
R(3)
HITRAN2020
This Work
S [cm-1/(molecule·cm-2)]
Temp.(K)
Temp.(K)
10-23
10-24
10-25
100
200
300

Fig.5b

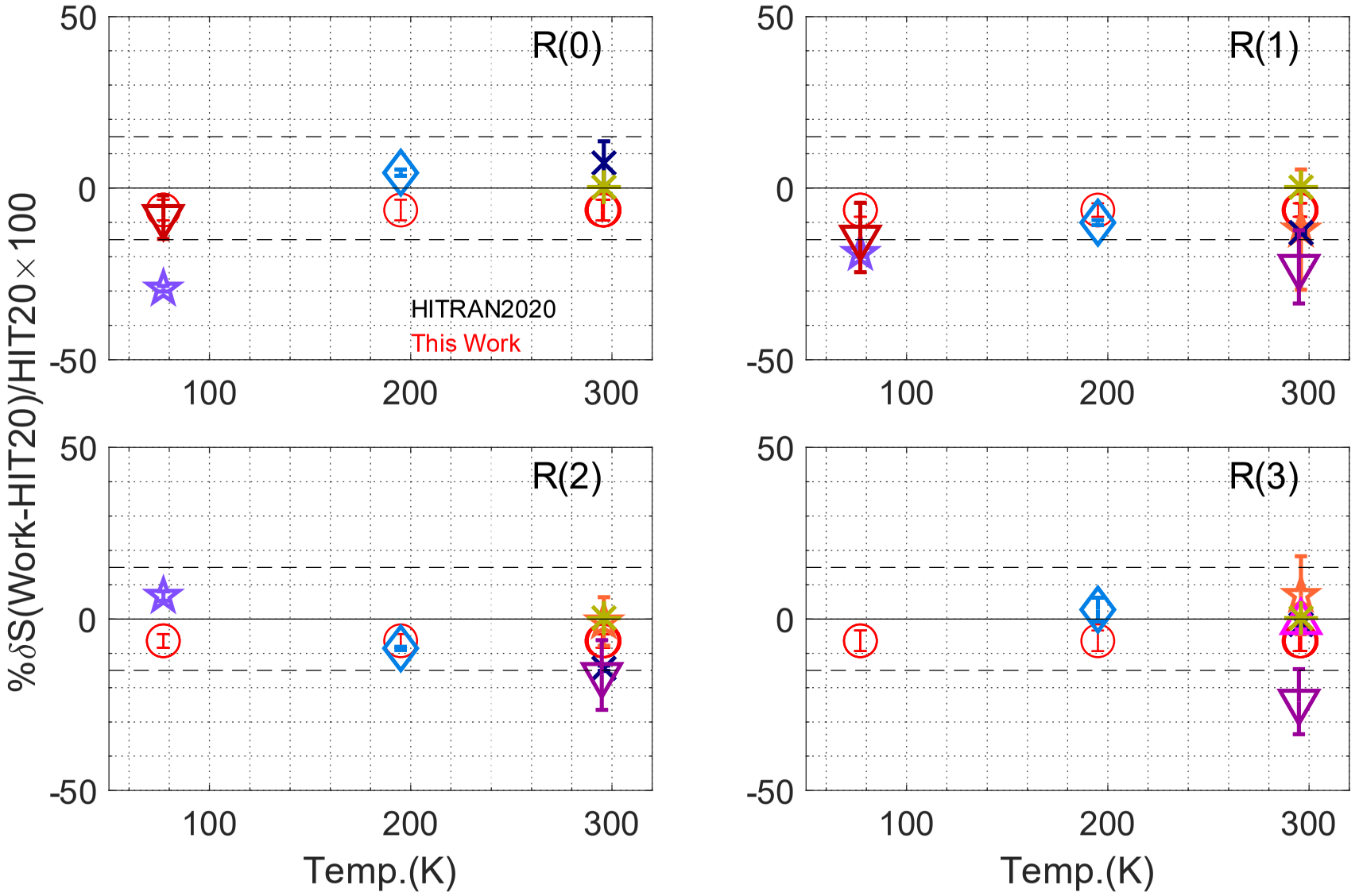
R(0)
R(1)
R(2)
R(3)
HITRAN2020
This Work
%δS(Work-HIT20)/HIT20×100
Temp.(K)
50
0
-50
100
200
300

Fig.6a

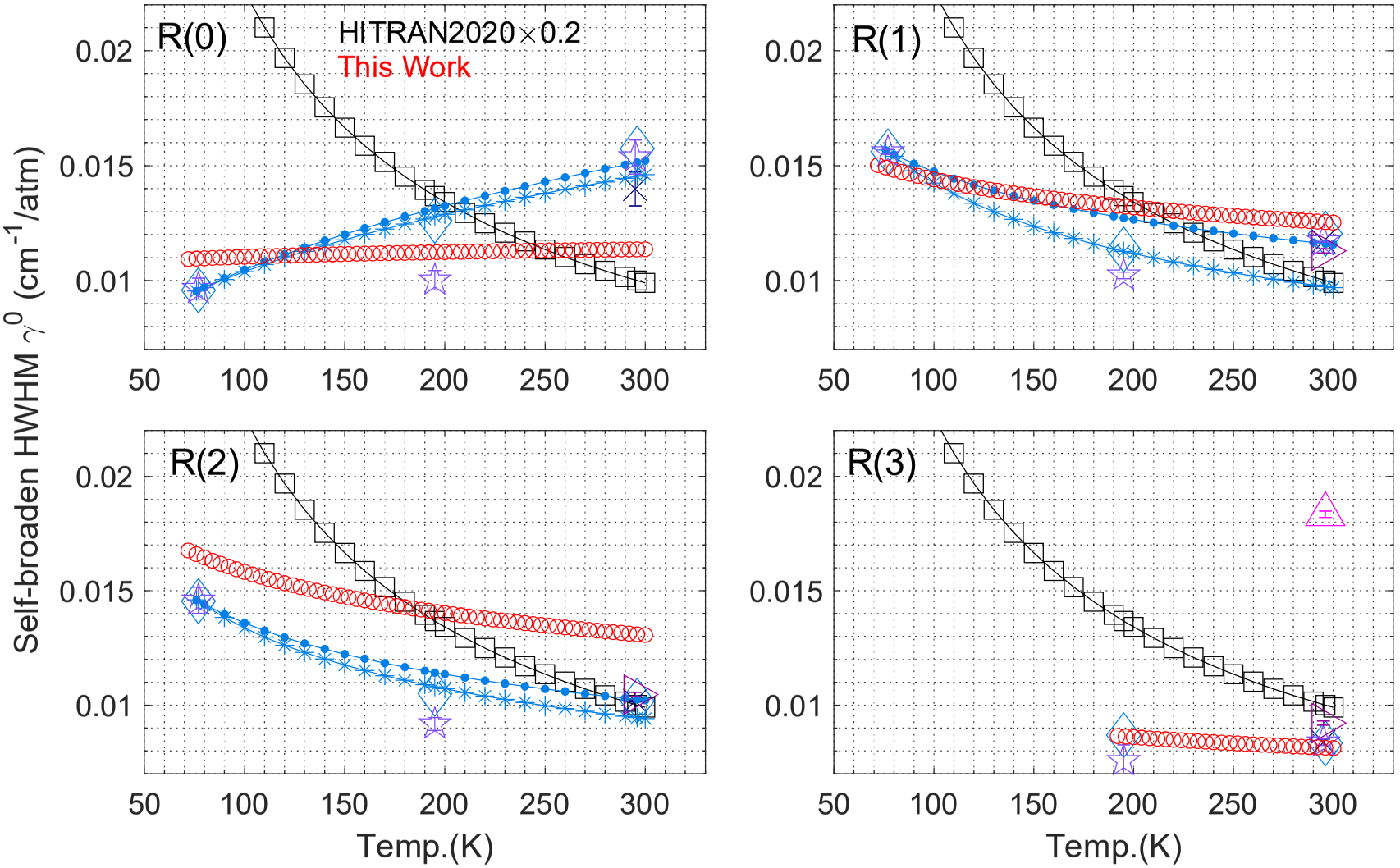
R(0)
HITRAN2020×0.2
This Work
R(1)
R(2)
R(3)
Self-broaden HWHM γ^0 (cm^{-1}/atm)
Temp.(K)
0.02
0.015
0.01
50
100
150
200
250
300

Fig.6b

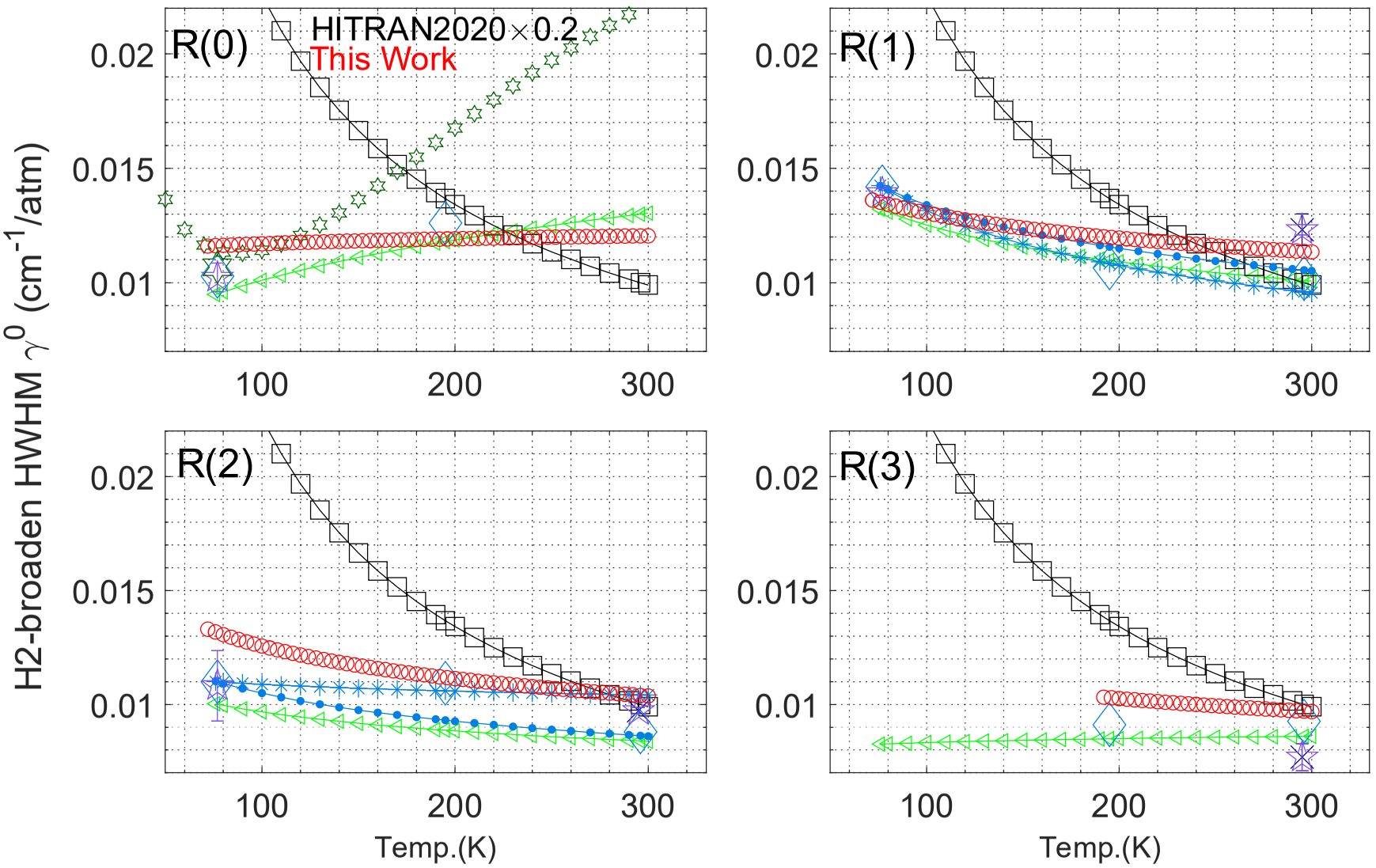
R(0)
HITRAN2020×0.2
This Work
R(1)
R(2)
R(3)
H2-broaden HWHM γ^0 (cm^{-1}/atm)
0.02
0.015
0.01
100
200
300
Temp.(K)

Fig.7a

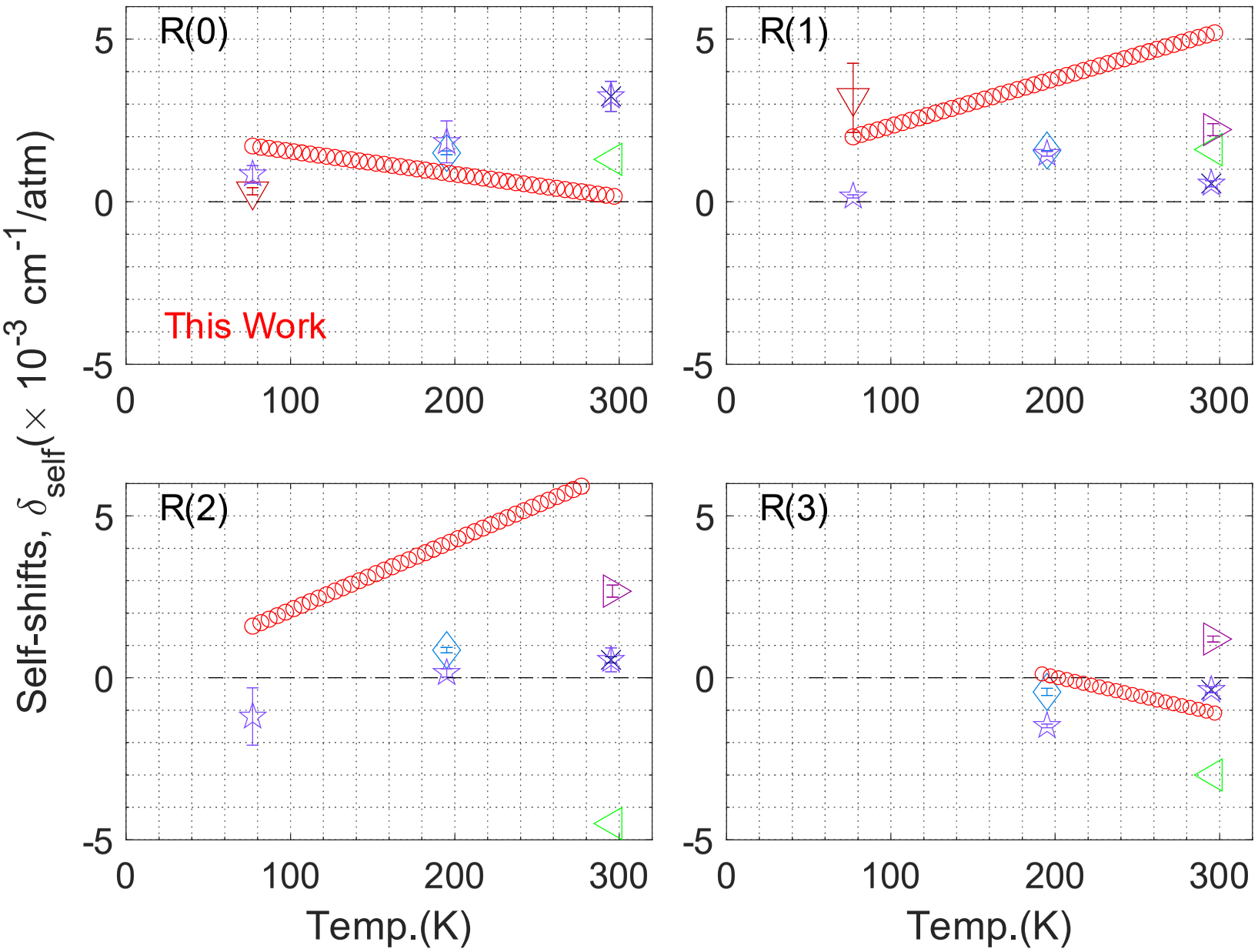
R(0)
R(1)
R(2)
R(3)
This Work
Self-shifts, δ_{self}($\times 10^{-3}$ cm^{-1}/atm)
Temp.(K)
Temp.(K)
5
0
-5
0
100
200
300

Fig.7b

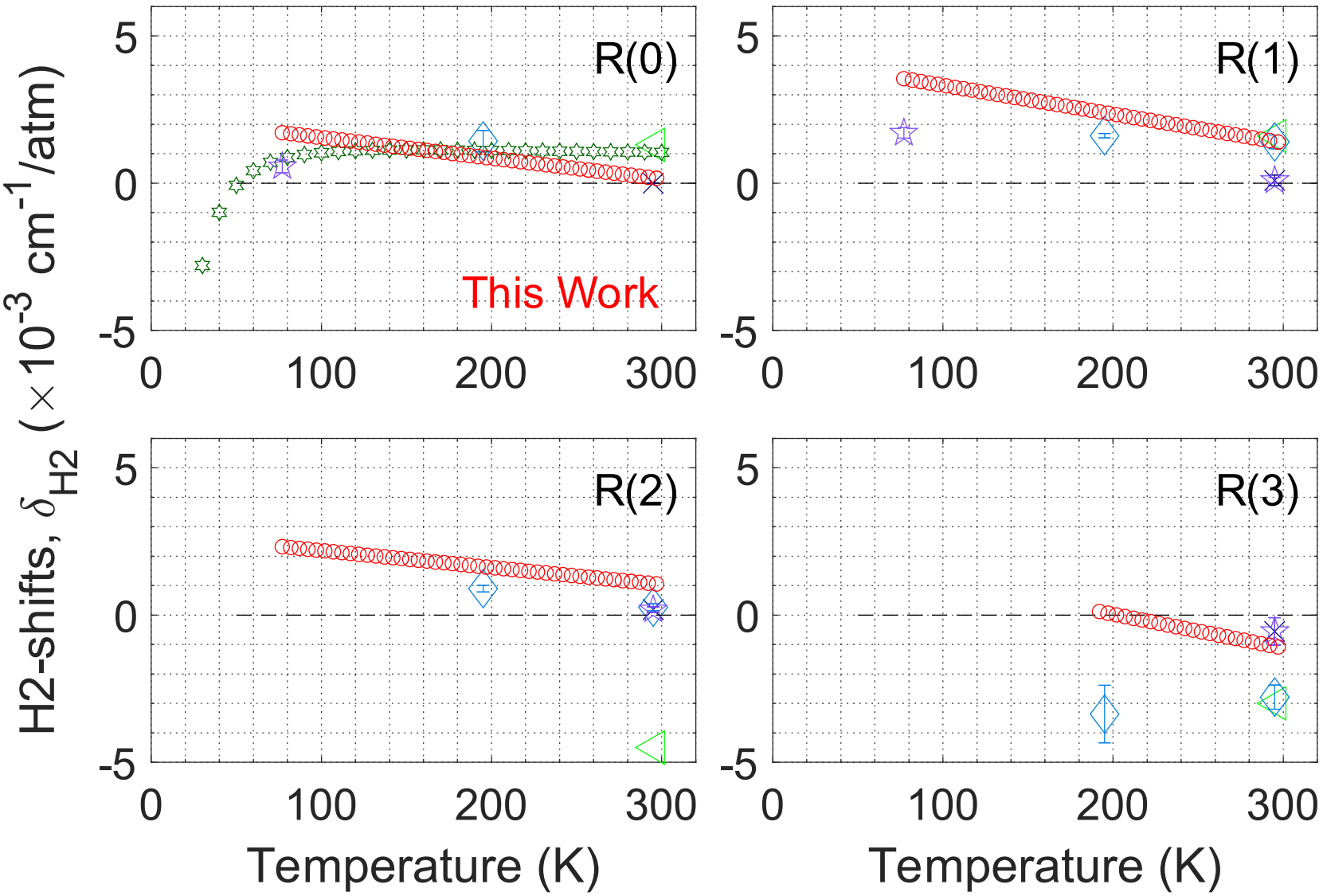
R(0)
R(1)
R(2)
R(3)
This Work
H2-shifts, δ_{H2} ($\times 10^{-3}$ cm^{-1}/atm)
Temperature (K)
Temperature (K)
5
0
-5
0
100
200
300

Fig.8a

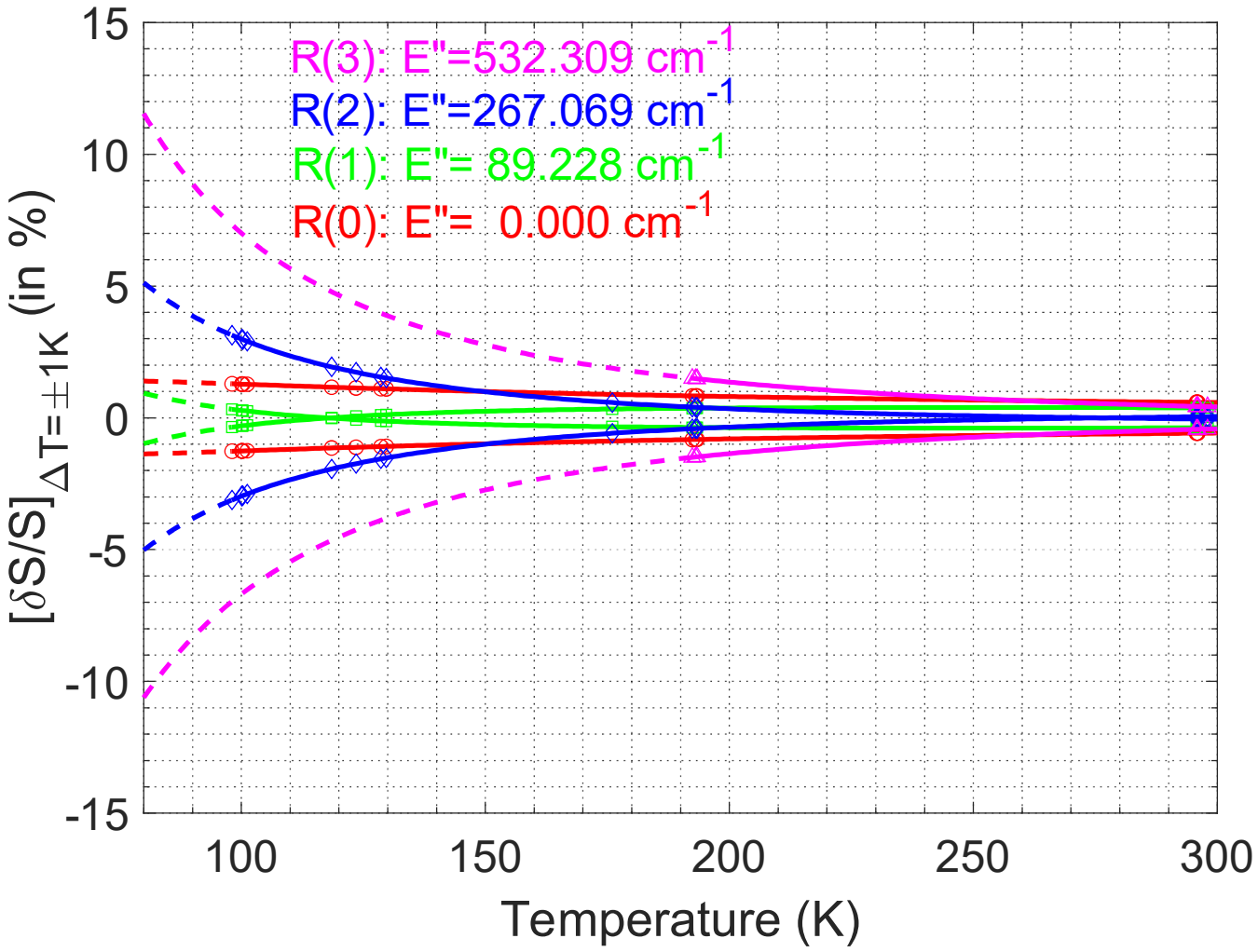
R(3): E"=532.309 cm-1
R(2): E"=267.069 cm-1
R(1): E"= 89.228 cm-1
R(0): E"= 0.000 cm-1
[δS/S]ΔT=±1K (in %)
Temperature (K)
15
10
5
0
-5
-10
-15
100
150
200
250
300

Fig.8b

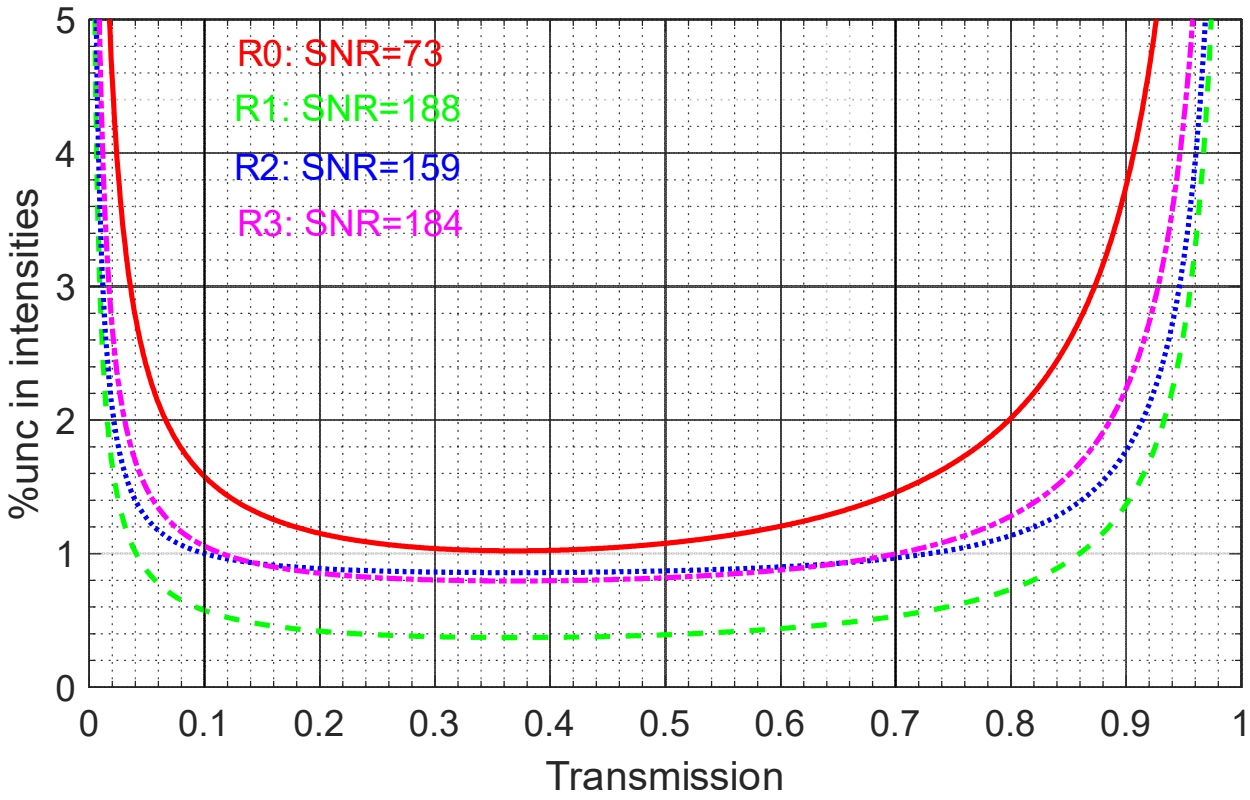
R0: SNR=73
R1: SNR=188
R2: SNR=159
R3: SNR=184
%unc in intensities
Transmission
0
1
2
3
4
5
0
0.1
0.2
0.3
0.4
0.5
0.6
0.7
0.8
0.9
1

Fig.9a

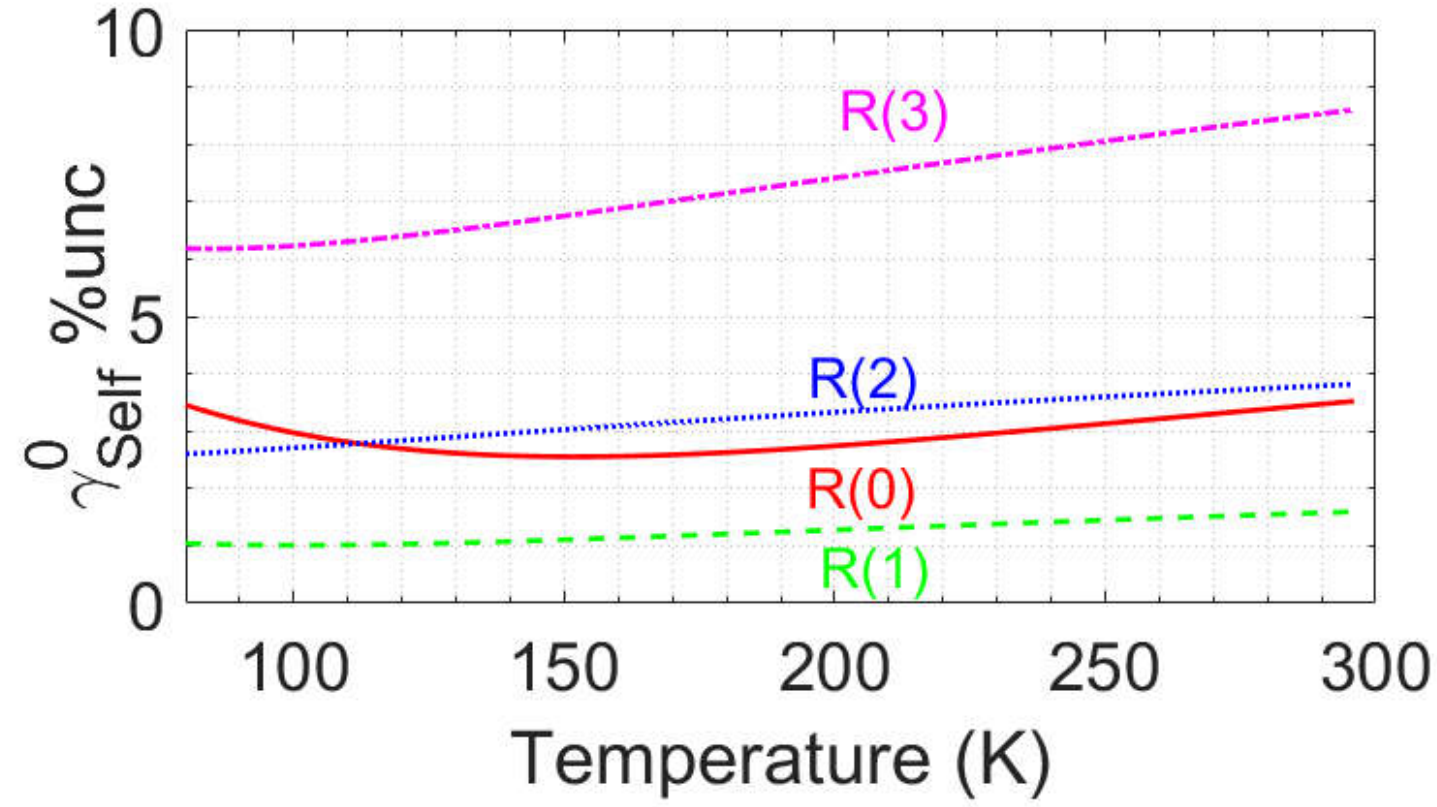
10
5
0
γ^0_{Self} %unc
R(3)
R(2)
R(0)
R(1)
100
150
200
250
300
Temperature (K)

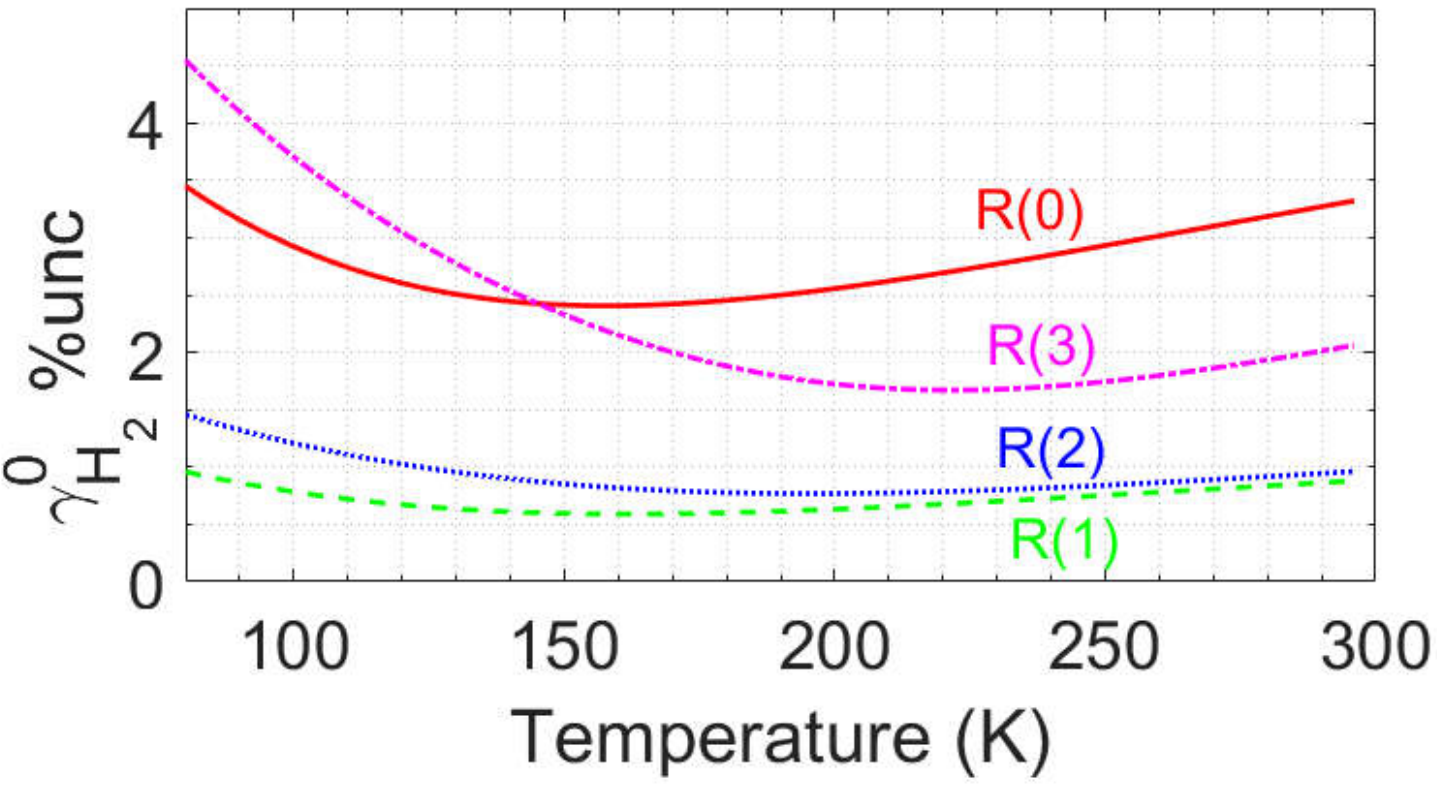
4
2
0
$\gamma^0_{H_2}$ %unc
R(0)
R(3)
R(2)
R(1)
100
150
200
250
300
Temperature (K)

Fig.9b

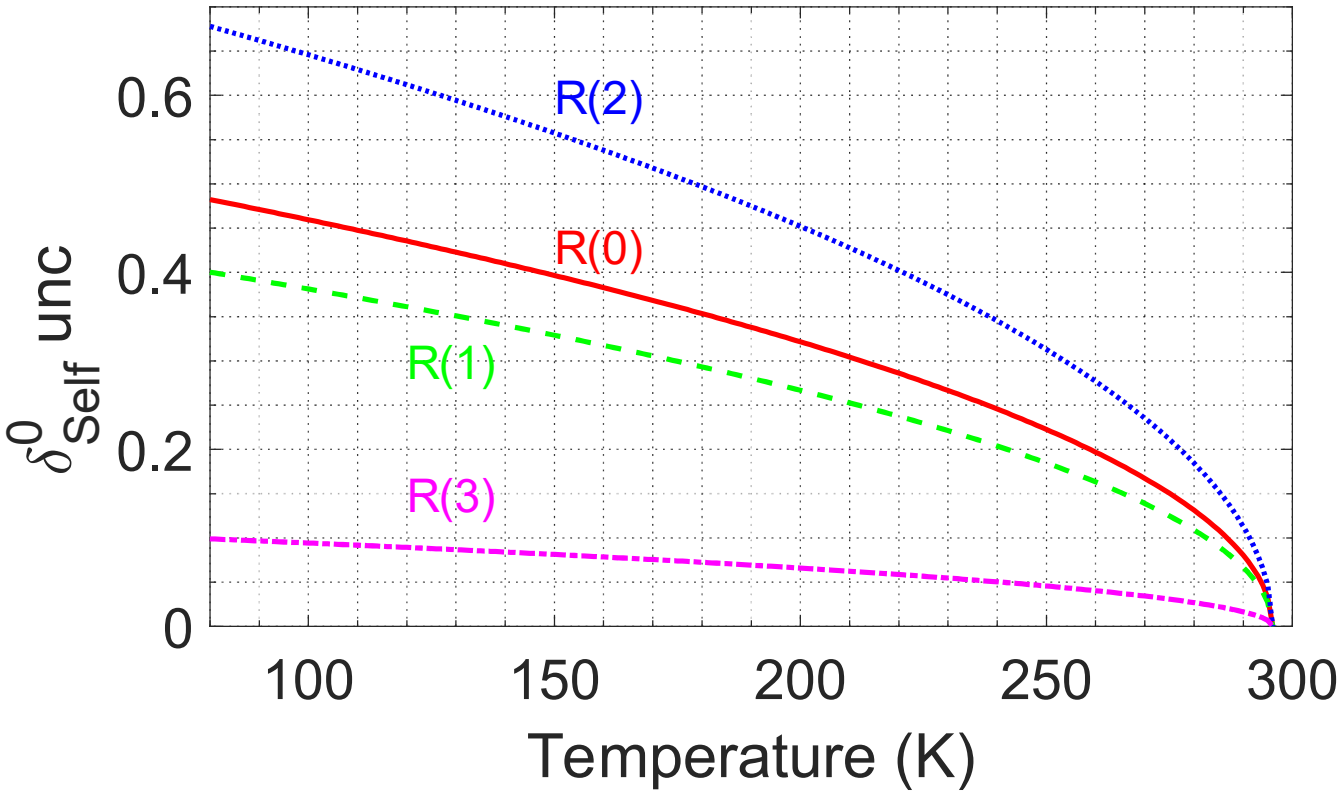
R(2)
R(0)
R(1)
R(3)
0.6
0.4
0.2
0
100
150
200
250
300
Temperature (K)
δ^0_{Self} unc

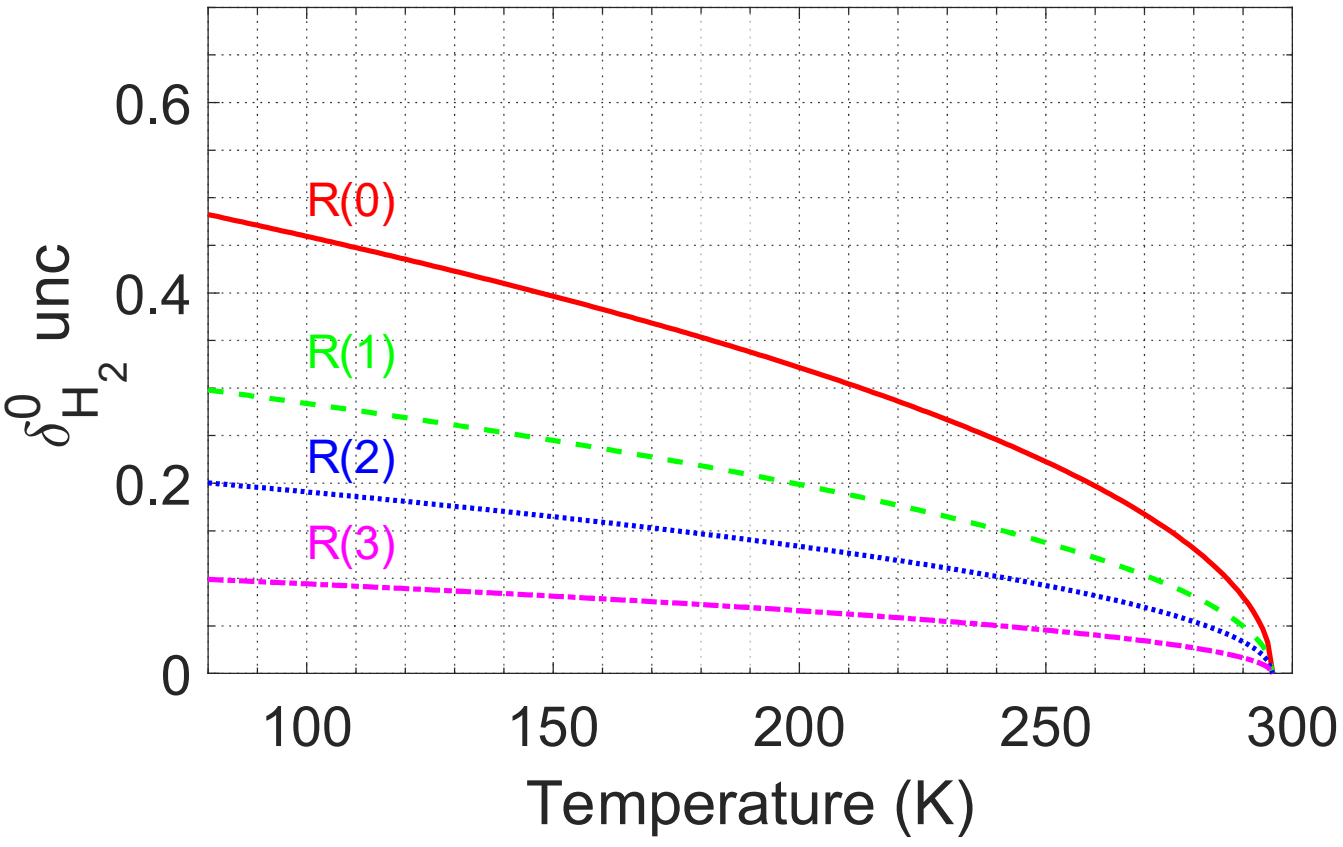
R(0)
R(1)
R(2)
R(3)
0.6
0.4
0.2
0
100
150
200
250
300
Temperature (K)
$\delta^0_{H_2}$ unc

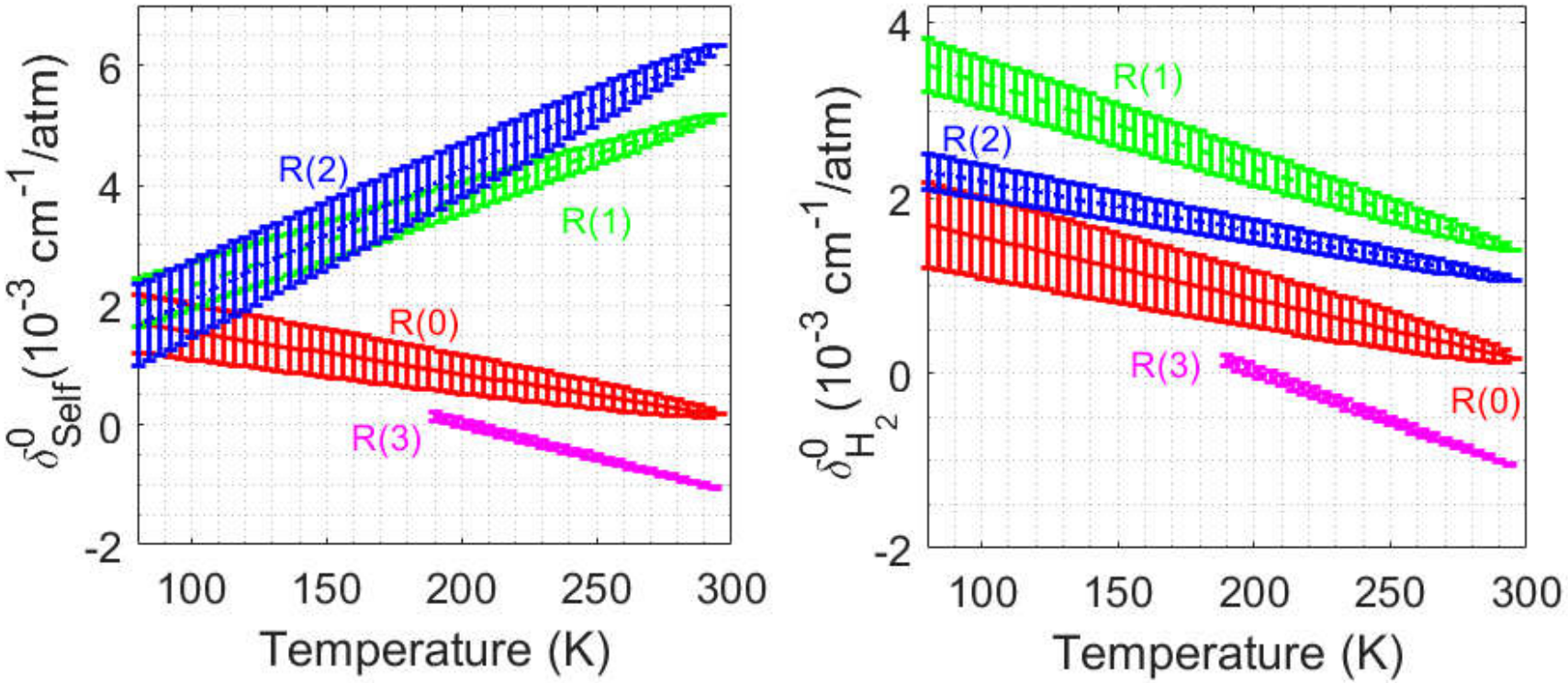
$\delta^0_{Self}(10^{-3}$ cm^{-1}/atm)
6
4
2
0
-2
R(2)
R(1)
R(0)
R(3)
100
150
200
250
300
Temperature (K)
$\delta^0_{H_2}$ $(10^{-3}$ cm^{-1}/atm)
4
2
0
-2
R(1)
R(2)
R(3)
R(0)
100
150
200
250
300
Temperature (K)

Conflict of Interest

Declaration of interests

☒The authors declare that they have no known competing financial interests or personal relationships that could have appeared to influence the work reported in this paper.

☐The authors declare the following financial interests/personal relationships which may be considered as potential competing interests:

CRediT authorship contribution statement

Keeyoon Sung - Conceptualization, Data acquisition, Data analysis, Visualization, Writing – original draft

Edward H. Wishnow - Conceptualization, Data acquisition, Writing, Proof-reading

Brian J. Drouin – Conceptualization, Proof-reading

Laurent Manceron, Data acquisition, Data analysis, Proof-reading

Marine Verseils, Data acquisition

D. Chris Benner - Software

Conor A. Nixon – Conceptualization, Proof-reading